

# Uncertainty Estimation for Novel Views in Gaussian Splatting from Primitive-Based Representations of Error and Visibility

Thomas Gottwald  
Department of Mathematics  
University of Wuppertal  
Wuppertal, Germany  
gottwald@uni-wuppertal.de

Edgar Heinert  
Department of Mathematics  
University of Wuppertal  
Wuppertal, Germany  
heinert@uni-wuppertal.de

Matthias Rottmann  
Institute of Computer Science  
Osnabrück University  
Osnabrück, Germany  
matthias.rottman@uos.de

## Abstract

*In this work, we present a novel method for uncertainty estimation (UE) in Gaussian Splatting. UE is crucial for using Gaussian Splatting in critical applications such as robotics and medicine. Previous methods typically estimate the variance of Gaussian primitives and use the rendering process to obtain pixel-wise uncertainties. Our method establishes primitive representations of error and visibility of training views, which carries meaningful uncertainty information. This representation is obtained by projection of training error and visibility onto the primitives. Uncertainties of novel views are obtained by rendering the primitive representations of uncertainty for those novel views, yielding uncertainty feature maps. To aggregate these uncertainty feature maps of novel views, we perform a pixel-wise regression on holdout data. In our experiments, we analyze the different components of our method, investigating various combinations of uncertainty feature maps and regression models. Furthermore, we considered the effect of separating splatting into foreground and background. Our UEs show high correlations to true errors, outperforming state-of-the-art methods, especially on foreground objects. The trained regression models show generalization capabilities to new scenes, allowing uncertainty estimation without the need for holdout data.*

## 1. Introduction

Recent volume-rendering-based methods that learn to represent the radiance field, a function that maps 3D positions and viewing directions to observed appearance, have advanced the state of the art in novel view synthesis and 3D reconstruction. Neural radiance fields (NeRFs) [23] use neural networks (NNs) for volume rendering, leveraging its differentiability to enable supervision from a set of posed camera views [13, 22, 44]. In Gaussian splatting [14], NNs are

replaced by Gaussian primitives, i.e., 3D Gaussian distributions with learnable position, variance, and opacity. These Gaussian primitives are initialized from a sparse point cloud obtained by structure from motion (SfM) [33] and are optimized by means of a rendering loss. NeRF and Gaussian Splatting both achieve high visual quality [3, 43] while the latter provides faster rendering and a more explicit representation of the scene [14, 21].

Gaussian Splatting (GS) faces similar challenges as NeRF-based methods. A major issue is that the positions of Gaussian splats oftentimes do not align with scene geometry, even when the radiance field’s appearance seems correct [8, 27, 37]. We refer to the discrepancy between the actual scene geometry and the spatial distribution of splats as the *depth error*. Furthermore, from the rendering process of a novel view alone it is unclear whether the resulting rendered image provides a reasonable approximation to the true scene and where it might be inaccurate [1, 32, 35]. This visual mismatch is what we refer to as the *rendering error*. While rendering-error-based optimization has been shown to cause geometric misalignment when Gaussian initializations are relaxed [12], other recent works attempt to mitigate the lack of reliability of GS by correcting depth and rendering errors through geometry smoothing [38], improved rendering optimization [9], and co-pruning or co-regularization of inconsistent Gaussians [42].

Addressing this issue directly, uncertainty estimation (UE) techniques are developed to identify such high-error views as well as erroneous regions of views. UE can be leveraged to obtain reliable geometry information of the scene which is crucial for any critical application, for instance in a medical environment or robotics [17, 31, 36]. Selecting additional training views from directions with high uncertainty can improve the radiance field approximation and reduce the amount of training data required for GS [11, 32], or guide robotic path planning to enhance environmental mapping [11]. UE in GS is still an open chal-

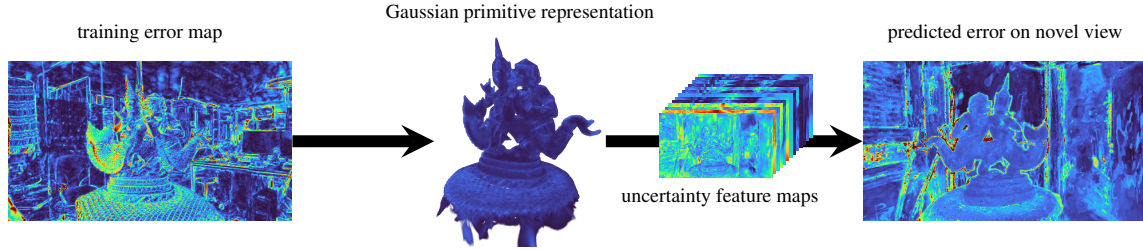


Figure 1. Our method uses the rendering error in the training views projected onto the Gaussian primitives as well as the Gaussian primitive visibility and field of view appearances in the training views. Based on those a set of Gaussian primitive representations are created, which can be rendered to novel views to give us a set of uncertainty feature maps. Via pixel-wise regression a prediction of the error in the view is created, which can be used as uncertainty measure. Further visual examples are illustrated in Appendix D.

lenge. Existing methods often estimate the uncertainty of individual Gaussian primitives and then use the standard GS rendering for uncertainty maps on pixel level [11, 39]. Therein, the uncertainty of a Gaussian is estimated either using Fisher information [11], or by learning some distribution for the Gaussian primitives [1, 39]. Whether uncertainties in the radiance field approximation yield depth or rendering error estimates [1] depends on the underlying method, the approximated scene geometry [11], semantic information integrated into GS [39].

In this work, we propose a UE method that provides Gaussian primitive representations of rendering errors and visibilities of Gaussians. These representations are constructed after a Gaussian splatting has been fitted to a given set of camera views. We model these representations with and without direction-dependency, studying camera-view-dependent UE. Each rendered representation yields a feature map for the given camera pose, which we call *uncertainty features*. Final uncertainty estimates are obtained by using gradient boosting to regress these features against rendering errors from one or a few novel views, yielding pixel-wise uncertainty maps.

In our numerical experiments, we study different numbers of views to train regression models, from one or multiple scenes, where training on just one view shows already promising results. The regression models generalize well to novel views of training scenes, achieving high correlation with the true error, and even generalize to novel scenes with moderately high Pearson correlation. Additionally, we segment the scenes into central foreground object and background regions. On foreground objects we observe higher correlation with the true error as well as improved generalization across scenes.

We summarize our contributions:

- We introduce a new state-of-the-art method for estimating pixel-wise uncertainty in GS reconstructions of RGB views and depth.
- We conduct an extensive ablation study on candidate feature maps, reducing them to a compact set of key features

that are most informative for UE.

- On two datasets and for both depth and rendering, our UE achieves high Pearson correlation with the true error on novel views and moderate generalization to novel scenes, consistently outperforming the FisherRF [11] baseline.

## 2. Related Work

In this section, we provide an overview of UE in NeRF and GS, the most recent approaches to novel view estimation.

**Uncertainty estimation for NeRFs** The uncertainty of NeRF is typically represented on pixel-level for a given camera view, i.e., an intermediate stage uncertainty representation like in a Gaussian primitive fashion is not available. In [30, 32], uncertainty is represented by stochastic radiance fields from which it can be estimated via sampling and estimating pixel-wise variance. On the other hand, [35] utilizes an ensemble of NNs for the sampling and determination of pixels’ variances. Extending the above mentioned works to GS is not straight-forward due to the difference in the radiance field representation. Other UE works for NeRF include uncertainty calibration [2] to improve the quality and interoperability of the predicted uncertainties. In [20], UE is performed on the training views to mask out inconsistencies and allow training on images from multiple sources. The latter has also been transferred to GS [16]. The last two works focus either on UE for the training data or on improving a given UE, while our work focuses on the estimation of uncertainties of the radiance field approximation in GS. Nonetheless, the existence of the discussed works underlines the research interest in UE for novel view estimation.

**Uncertainty estimation for Gaussian splatting** For UE in GS, most methods consider uncertainties on the level of Gaussian primitives. Utilising a Bayesian postprocessing approach, Wilson et al. [39] incorporate semantic information into the Gaussian representations. To this end, they

learn a distribution over semantic classes for the Gaussian primitives, using its variance to perform uncertainty estimation with respect to scene semantics. With a stochastic radiance field method, Aria et al. [1] learn the distribution of the Gaussian primitive parameters using a Gaussian prior distribution and the Bayesian update rule. Then, pixel uncertainties are estimated via the variance of multiple sample renderings. In a preprint [6], direction-dependent uncertainty is modeled directly during Gaussian Splatting (GS) training. Jiang et al. [11] use the Fisher information matrix to obtain parameter variances. The methods [11, 39] can provide pixel-wise uncertainties via Gaussian Splatting rendering process by replacing color with Gaussian primitive uncertainty, i.e. either semantic or aggregated parameter variances. In contrast to [1, 6], our UE operates purely as a post-processing step, without interfering with the Gaussian Splatting training. It requires only a few views to fit the uncertainty regression and generalizes to novel scenes without access to their GS training data. Compared to the post-processing approach by Jiang et al. [11], which relies on a single uncertainty representation, we extract 13 optionally direction-dependent feature maps per Gaussian, based on training view visibility and reconstruction error. Lightweight gradient boosting is trained on the rendered 2D features to estimate depth and rendering error, consistently outperforming their method.

### 3. Method

In this section, we review Gaussian Splatting volume rendering, which is then used to introduce our Gaussian primitive representations. We describe the construction of those representations and explain how the rendered uncertainty feature maps are used for UE in novel view estimation.

**Gaussian Splatting** GS provides an approximation of the radiance field via Gaussian primitives. These Gaussian primitives are given as scaled 3D Gaussian distributions with mean  $\mu$ , covariance matrix  $\Sigma$ , a scalar opacity factor  $g$  and color  $c$ . To render a view, given by position, direction  $\vec{d}$  and camera intrinsics, in the first step all Gaussian primitives are sorted from front to back and then projected onto the camera plane. This projection, also called splatting [44], converts the 3D Gaussian distributions of the Gaussian primitives to 2D ones on the camera plane. The opacity of a Gaussian primitive at pixel  $\bar{x}$  of a view is then given as

$$\alpha(\bar{x}) = g\Phi(\bar{x}; \bar{\mu}, \bar{\Sigma}), \quad (1)$$

with  $\bar{\mu}$  and  $\bar{\Sigma}$  the mean and covariance matrix of the 2D Gaussian distribution. The final color at the pixel is obtained via the aggregation from front to back of the sorted

Gaussian primitives

$$C(\bar{x}) = \sum_{k=1}^K c_k(\vec{d})\alpha_k(\bar{x})T_k(\bar{x}), \quad (2)$$

with  $c_k(\vec{d})$ ,  $\alpha_k(\bar{x})$  the opacity and color of the  $k$ th Gaussian primitive and  $T_k(\bar{x}) = \prod_{j=1}^{k-1} (1 - \alpha_j(\bar{x}))$  the transparency of the volume from Gaussian primitive 1 to  $(k-1)$ . The color of the Gaussian primitives depends on the direction  $\vec{d}$  of the view. This view dependence is realized using spherical harmonics, which are common to encode signals on spheres [24, 26]. GS learns the parameters of the Gaussian primitives, i.e. mean, covariance matrix, opacity factor and color, via gradient descent, where the gradients of the reconstruction loss w.r.t. the Gaussian primitive parameters are computed for a set of training views.

**Gaussian Primitive Representations** Our Gaussian primitive representations are based on both the visibility of Gaussian primitives and the rendering error in training views. Therefrom, we capture uncertainty arising from limited coverage in the training data as well as from imperfect optimization. We start with a simple representation where we count how often a Gaussian primitive appears in the field of view (FoV) of the training views. For that, we consider a Gaussian primitive to bin the FoV of a view if its mean lies in a slightly extended version of the view cone. Formally, the FoV counter for the  $k$ th Gaussian primitive is given by

$$F(k) = |\Omega_k|, \quad (3)$$

with  $\Omega_k$  the set of training views in which the  $k$ th Gaussian primitive appears in the FoV. Another type of Gaussian primitive representation that we propose represents the visibility of Gaussian primitives in the training views. Additionally, we propose two Gaussian primitive representations that represent the visibility and rendering error contribution of the Gaussian primitives for the training views. For the visibility of a Gaussian primitive in a training view we consider the contribution factors, i.e.  $\alpha_k(\bar{x})T_k(\bar{x})$  from Eq. (2), of the Gaussian primitive in each pixel of the training view. This contribution factors are then aggregated over all pixels in the view where the Gaussian primitive is visible considering different aggregation functions  $\text{agg} \in \{\text{max}, \text{sum}, \text{mean}\}$ . We chose the limitation to pixels where the Gaussian primitive is visible to get appropriate visibilities for Gaussian primitives of different sizes when using mean aggregation. As final training visibility of a Gaussian primitive we select the maximum of the aggregated contribution factors, with the intuition that a Gaussian only needs to be highly visible in a few training views to be well observed. Training visibility representation (short: vis-

ibility representation) is defined as

$$V(k) = \max_{v \in \Omega} \text{agg}_{\bar{x} \in v(k)} \alpha_k(\bar{x}) T_k(\bar{x}), \quad (4)$$

with  $v(k)$  denotes the set of pixels from training view  $v \in \Omega$  in which the the opacity of the  $k$ th Gaussian primitive is visible. The representation for the rendering error contributed by the Gaussian primitives is defined similarly to the visibility representation. We add the reconstruction error of the pixels in the training views as factor to the contributing term in the aggregation. Additionally, we choose the mean over the training views of the aggregated terms for our training reconstruction error representation (short: error representation). Formally, for the  $k$ th Gaussian primitive

$$E(k) = \text{mean}_{v \in \Omega} \text{agg}_{\bar{x} \in v(k)} e_{\bar{x}} \alpha_k(\bar{x}) T_k(\bar{x}), \quad (5)$$

with  $e_{\bar{x}}$  the reconstruction error value at pixel  $\bar{x}$  of the view  $v$ . For both the visibility and the error representation we consider different aggregation functions to capture different uncertainties. Additionally, we also consider the option to drop the opacity  $\alpha_k(\bar{x})$  (Eq. (1)) in the Eqs. (4) and (5) for visibility and the error representation. Our intuition is that a Gaussian primitive with a low opacity might still be well visible or responsible for a high reconstruction error in a pixel of the training views but without dropping opacity it would barely contribute to pixel-wise uncertainty features.

**Direction-Dependent Representation** We have the choice to make the representations of visibility and error direction-dependent, e.g. not only considering how visible a Gaussian primitive is but also from which directions it is well visible in the training views. To model the direction dependency we use the von Mises-Fisher distribution [5, 19], which can be seen as the Normal distribution on hyper spheres. For a 3D sphere its density is defined as

$$f(\vec{x}; \vec{\nu}, \kappa) = \frac{\kappa}{2\pi \sinh(\kappa)} \exp(\kappa \vec{\nu}^\top \vec{x}), \quad (6)$$

with  $\vec{\nu}, \vec{x} \in \mathbb{S}^2$  (vectors on the sphere), where  $\vec{\nu}$  is the mean direction, and  $\kappa$  a scaler determining the spread of the distribution. We use a rescaled version of the density to have a maximum value of one that is multiplied to the terms in the aggregation of Eqs. (4) and (5). Formally, the direction-dependent visibility and error representations are given by

$$V^*(k, \vec{d}) = \max_{v \in \Omega} \text{agg}_{\bar{x} \in v(k)} \alpha_k(\bar{x}) T_k(\bar{x}) \exp(\kappa \vec{\nu}_v^\top \vec{d} - \kappa) \quad (7)$$

$$E^*(k, \vec{d}) = \text{mean}_{v \in \Omega} \text{agg}_{\bar{x} \in v(k)} e_{\bar{x}} \alpha_k(\bar{x}) T_k(\bar{x}) \exp(\kappa \vec{\nu}_v^\top \vec{d} - \kappa), \quad (8)$$

with  $\vec{\nu}_v$  the direction of the view  $v$  and  $\vec{d}$  the direction for which we evaluate the representation. The process of making the representations direction dependent can be seen as

placing for each Gaussian primitive a rescaled von Mises-Fisher distribution (such that its peak has a “density” of 1) on a sphere at the positions corresponding to the training views. To facilitate rendering of the representations, we encode them using spherical harmonics, which GS already uses to encode the Gaussian primitive color values.

**Regression Models** To obtain pixel-wise uncertainties for a novel view, we render a set of chosen uncertainty feature maps based on the Gaussian primitive representations by replacing Gaussian primitive color with the respective Gaussian primitive representation in the GS rendering Eq. (2). To aggregate the uncertainty feature maps into a single uncertainty measure, we use a pixel-wise regression model. Aggregating and analyzing our uncertainty feature maps based on regression analysis is also inspired by a line of works in object detection as well as semantic and instance segmentation [4, 7, 15, 18, 28, 29]. The regression model is trained on a set of hold-out views to predict the rendering or the depth error based on the uncertainty feature maps. The target of the regression model in rendering or depth error for a pixel  $\bar{x}$  is defined as

$$e_{\bar{x}} = ||R(\bar{x}) - \hat{R}(\bar{x})||_1, \quad (9)$$

with  $R(\bar{x})$  and  $\hat{R}(\bar{x})$  the ground truth and rendered view of color or depth, respectively. In principle one could use different distance measures to define the error but GS typically uses the L1-norm in its loss function.

## 4. Numerical Results

In this section, we first give an overview of the experimental setup, where we introduce the used scene datasets, state the specifics of the method, introduce our base setup for pixel-wise UE and the evaluation metrics we used. Then, we present our experiments and their numerical results: We compare the in-scene generalization of our UE methods with standard FisherRF and an improved variant. We then conduct an ablation to study the importance of each uncertainty feature through greedy feature removal. Next, we evaluate out-of-scene generalization of our UE. Finally, we explore the usefulness of uncertainty feature-map pixel neighborhoods for UE using convolutional networks. Extended per-scene results for in-scene and out-of-scene generalization are provided in Appendix B and C. We visualize predicted and true uncertainties in Appendix D.

**Experimental Setup** For UE estimation, we use 4 object-centric scenes from the Light Field (LF) [32, 41] and 11 from the the RGB-D SLAM dataset from TU Munich (short TUM dataset) [34], each featuring a camera trajectory circling around a central object. Both include ground truth depth for selected hold-out views. TUM scenes, sourced



from a SLAM benchmark, involve two to three camera rotations at varying heights and often contain motion blur, leading to higher rendering errors compared to LF.

As uncertainty feature maps we use an FoV counter feature map (short FoV counter), 6 visibility feature maps (short visibility maps) and 6 error feature maps (short error representation maps), which are based on the FoV counter, visibility and error representation, respectively. For the FoV counter feature map, we use the standard clipping of Gaussian primitives during rendering used in the GS implementation [14]. The 6 visibility and 6 error feature maps are both combined with the aggregation functions max, sum and mean, each of them once including  $\alpha_k$  and once dropping  $\alpha_k$  from Eqs. (4) and (5). For the aggregation over pixels we use the standard GS process to decide whether a Gaussian primitive is visible in a pixel, i.e., whenever  $\alpha_k(\bar{x}) \geq \frac{1}{255}$  and  $T_k(\bar{x}) \geq 10^{-3}$ . Additionally, we also use the visibility and error feature maps based on the direction-dependent versions of the Gaussian primitive representations (Eqs. (7) and (8)). There we consider  $\kappa = 8$  for the rescaled von Mises-Fisher distribution and a spherical harmonics degree of four, which performed well in our experiments. The distributions spread over the sphere but still leave room for direction-dependent representations.

If not stated otherwise, we perform pixel-wise UE via gradient boosting regression [25] to predict the rendering or depth error by means of all 13 direction-independent uncertainty feature maps, i.e., the FoV counter, 6 visibility and 6 error feature maps. The regression model is trained on a single hold-out view of a scene. Rendering and depth error are learned by two separate gradient boosting models. We trained additional regression models for a separation of the Gaussian Splatting of the scenes in object and background, using the Gaussian Grouping method by Ye et al. [40].

**Evaluation Metrics** To evaluate the predictive performance of the uncertainty estimation, we use the Pearson correlation of the predicted error to the true error. For a fair comparison to FisherRF we also investigate the area under sparsification error (AUSE) [10] based on the mean absolute error (MAE). The AUSE metric is defined as the area between two filtration curves, which depict the development of the mean error (here MAE) when a fraction of the pixels with highest error or, respectively, highest uncertainty is removed. When the considered uncertainty estimation correlates well to the error, both filtration curves align and leave only a small area between them, resulting in low AUSE scores. To compute the AUSE metric evaluated on different views, we rescale the total error of the view to one. We choose Pearson correlation over AUSE as our main evaluation metric due to its suitability to the regression task and for its simplicity and interpretability. We refrained from standard regression evaluation metrics like the coefficient of

determination ( $R^2$ ), due to a potential shift in ranges of input or target for the regression for a novel view. Such shifts also occur for novel views from the same scene as the hold-out views that the regression model was trained on.

**FisherRF Baselines** As a baseline, we consider FisherRF by Jiang et al. [11], which estimates Gaussian primitive uncertainty via the diagonal of the Fisher information matrix. In addition to the original method, we include a modified variant using six grouped parameter-based uncertainty feature maps, making it more comparable to our approach. Full details are provided in Appendix A.

**In-Scene Uncertainty Estimation** In our in-scene UE study, for each scene we train regression models on one or multiple hold-out views of the respective scene and evaluate the UE on a set of different hold-out views of the respective scene. As sets of uncertainty feature maps, we consider 1) all 13 direction-independent maps; 2) selected subsets of those 13 maps based on our feature selection study (presented later); 3) all 12 direction-dependent maps along with the FoV counter map. We compare our results to FisherRF UE and regression models trained on the 6 FisherRF uncertainty feature maps (regression-FisherRF). Additionally, we compare linear regression and gradient boostings. Across (LF and TUM), training regimes (1-view and multi-view), target variables (depth and rendering error), and considered metrics (AUSE score and Pearson correlation), we observe several consistent trends. Our methods outperform both standard FisherRF and regression-FisherRF, with the latter consistently improving over the former. Gradient boosting outperforms linear regression in most settings, indicating a nonlinear relationship between the uncertainty features and prediction targets. Using more uncertainty feature maps and more training views consistently improve UE. Direction-dependent features are slightly beneficial on LF but not effective or detrimental on TUM, particularly when focusing on the central object. These trends hold for both full-scene and object-centric evaluations, unless noted otherwise.

Table 1 reports AUSE scores for each LF image and scene-level averages for LF and TUM. AUSE, the primary metric used by Jiang et al. [11], measures correlation between predicted uncertainty and true depth error. Direction-dependent feature maps offer a slight advantage on LF, while direction-independent maps perform clearly better on TUM. Interestingly, on the LF scene \*torch\*, regression-FisherRF slightly outperforms our method which still improves substantially over standard FisherRF. Table 2 presents Pearson correlations between predicted and true depth and rendering error. For depth UE, FisherRF shows a moderate negative correlation with the true error on TUM; however, our UE still outperforms it when considering absolute correlation values. Notably, on TUM single-view

views	method	no. of maps	metric dataset scene model	AUSE ↓					
				africa	basket	statue	torch	LF mean	TUM mean
1-view	FisherRF			0.392	0.316	0.201	0.38	0.322	0.742
	reg. FisherRF	6	grad.	0.17	0.131	0.108	<b>0.124</b>	0.133	0.328
			lin.	0.261	0.202	0.163	0.224	0.212	0.363
	vis. err. maps	13	grad.	0.13	0.098	0.076	0.145	0.112	0.213
			lin.	0.17	0.138	0.15	0.352	0.202	0.188
		9a	grad.	0.131	0.101	0.083	0.166	0.12	0.214
		9b	grad.	0.135	0.102	0.078	0.168	0.121	0.22
		9c	grad.	0.135	0.104	0.078	0.168	0.121	0.216
	vis. err. maps*	13	grad.	0.127	0.095	0.074	0.137	0.108	0.239
m-view			lin.	0.169	0.143	0.162	0.333	0.202	0.226
	reg. FisherRF	6	grad.	0.159	0.118	0.105	0.126	0.127	0.226
	vis. err. maps	13	grad.	0.116	0.081	0.067	0.13	<b>0.099</b>	<b>0.132</b>
	vis. err. maps*	13	grad.	<b>0.114</b>	<b>0.08</b>	<b>0.066</b>	0.129	<b>0.097</b>	0.161

Table 1. AUSE scores for UE of the depth error for entire scene evaluation. 1-view and m-view describe whether we use one or multiple views for UE regression (grad. for gradient boosting, lin. for linear regression).

training, linear regression surpasses gradient boosting, opposite to the trend observed on LF. For rendering UE, FisherRF slightly outperforms gradient boosting in the TUM single-view setup, though it is again surpassed by linear regression. On LF and in the multi-view TUM setup, gradient boosting yields the best results. Direction-dependent features consistently improve rendering UE, with gains ranging from moderate to substantial.

In addition to training UE on entire views, we evaluate regressors trained and tested exclusively on the central objects of views. Table 3 shows Pearson correlations between predicted and true depth and rendering error for this setting. For depth UE, our methods outperform both plain and regression FisherRF, reaching correlations up to 0.85 in the multi-view setup on both LF and TUM. Direction-dependent features offer no benefit, and reducing the feature maps to subsets (a–c) does not degrade performance. Gradient boosting consistently surpasses linear regression. Similar trends are observed for rendering UE: our methods outperform both FisherRF baselines across datasets and training setups. Again, gradient boosting performs best, while direction-dependent features slightly reduce performance on the central object.

**Uncertainty Feature Map Selection Study** To investigate which of our uncertainty feature maps carry the most information, we perform a step-wise backward regression. That is, we train regression models to predict the depth error, and, in a greedy manner, drop the uncertainty feature map that causes the least reduction in Pearson correlation to true errors. This is repeated until only a single uncertainty feature map remains. For this experiment, we only consider the gradient boosting regressors trained on a single view and evaluate them on the remaining hold-out views of the same scene (2 for LF, 3 for TUM). We selected the hold-out views of the LF dataset as well as 5 hold-out views from

views	method	no. of maps	predicted error type dataset scene model	depth error			rendering error		
				LF mean	TUM mean	mean	LF mean	TUM mean	mean
1-view	FisherRF			0.31	-0.08	0.115	-0.224	-0.241	-0.232
	reg. FisherRF	6	grad.	0.683	0.375	0.529	0.318	0.181	0.249
			lin.	0.452	0.305	0.378	0.182	0.143	0.162
	vis. err. maps	13	grad.	0.734	0.536	0.635	0.412	0.217	0.314
			lin.	0.545	0.571	0.558	0.309	0.29	0.3
		9a	grad.	0.721	0.536	0.628	0.407	0.222	0.314
		9b	grad.	0.716	0.525	0.621	0.408	0.216	0.312
		9c	grad.	0.708	0.535	0.622	0.402	0.211	0.307
	vis. err. maps*	13	grad.	0.739	0.501	0.62	0.419	0.23	0.324
m-view			lin.	0.557	0.521	0.539	0.35	0.296	0.323
	reg. FisherRF	6	grad.	0.715	0.515	0.615	0.352	0.267	0.31
	vis. err. maps	13	grad.	0.777	<b>0.653</b>	<b>0.715</b>	0.446	0.302	0.374
	vis. err. maps*	13	grad.	<b>0.788</b>	0.605	0.696	<b>0.458</b>	<b>0.321</b>	<b>0.389</b>

Table 2. Pearson Correlation of predicted to true depth/rendering error for entire scene evaluation. 1-view and m-view describe whether we use one or multiple views for UE regression (grad. for gradient boosting, lin. for linear regression).

views	method	no. of maps	predicted error type dataset scene model	depth error			rendering error		
				LF mean	TUM mean	mean	LF mean	TUM mean	mean
1-view	FisherRF			0.05	0.303	0.177	0.129	0.458	0.293
	reg. FisherRF	6	grad.	0.698	0.521	0.609	0.704	0.645	0.675
			lin.	0.398	0.364	0.381	0.404	0.523	0.463
	vis. err. maps	13	grad.	0.835	0.745	0.79	0.822	0.756	0.789
			lin.	0.707	0.586	0.646	0.633	0.617	0.625
		6a	grad.	0.822	0.736	0.779	0.807	0.747	0.777
		6b	grad.	0.822	0.744	0.783	0.8	0.75	0.775
		6c	grad.	0.832	0.746	0.789	0.811	0.75	0.78
	vis. err. maps*	13	grad.	0.831	0.718	0.774	0.818	0.724	0.771
m-view			lin.	0.612	0.435	0.523	0.526	0.526	0.526
	reg. FisherRF	6	grad.	0.757	0.7	0.728	0.751	0.766	0.759
	vis. err. maps	13	grad.	<b>0.859</b>	<b>0.849</b>	<b>0.854</b>	<b>0.842</b>	<b>0.851</b>	<b>0.847</b>
	vis. err. maps*	13	grad.	<b>0.859</b>	0.825	0.842	<b>0.842</b>	0.811	0.826

Table 3. Pearson Correlation of predicted to true depth/rendering error for object-centric scene evaluation. 1-view and m-view describe whether we use one or multiple views for UE regression (grad. for gradient boosting, lin. for linear regression).

5 scenes of the TUM dataset (pant, flower, metallic, dishes, cabinet) for the training of regression models. The initial set of uncertainty feature maps consists of the 13 direction-independent ones. Analogously, we perform an additional step-wise backward regression for the scenes limited to the central object. In Fig. 2 we provide the mean trajectories of the Pearson correlation scores over the steps of the step-wise backward regression depicted on the left. The bar chart shows for how many steps an uncertainty feature was used before being dropped. In the trajectory plots on the left we see that the UE performance is higher when considering the central object, and we have less variance in the score as indicated by the shaded region. We obtain noticeably lower scores when only few uncertainty feature maps remain. However, we the score first increases before it drops, which is due to overfitting to the given uncertainty feature maps. The optimal performance is achieved for about 9 uncertainty feature maps when considering the entire scenes and about 6 in the object-centric case. In particular, for the

object-centric case, a board plateau of high Pearson correlations indicates a low sensitivity to the number of uncertainty feature maps. The right-hand side of Fig. 2 shows how many steps (on average) a given uncertainty feature map survives before being dropped. The FoV counter survives for the most steps when evaluating on the whole scene and is still strong in the object-centric case. In the latter case, the visibility uncertainty feature map with max aggregation and dropped  $\alpha_k(\bar{x})$  in Eq. (4) survives just as long. Intuitively, the FoV counter is more important for full-scene depth UE than on the central object alone as the scenes are captured from views placed around and focused on the central objects. This naturally leads to high FoV counts for Gaussian primitives representing the central object, whereas across the full scene, variation in FoV counts is more indicative of depth errors. When we limit the UE to the central object, the FoV count may be less informative, as it is generally high across that region and lacks finer spatial variation. Here, one of the visibility-based uncertainty feature maps, which uses max aggregation and drops the opacity  $\alpha_k$  in Eq. (4), is similarly important. It highlights Gaussians with strong contributions in at least one training view, which often corresponds to broader influence across that view. The dropped opacity may reflect the importance of semi-transparent Gaussian primitives in shaping the predicted depth map in Gaussian Splatting. In contrast, none of the training error-based uncertainty feature maps rank highly in importance. This is likely due to those uncertainty feature maps being derived from reconstruction error during training, thus being less informative for depth UE.

Based on the general results of both step-wise backward regressions, we select different subsets of uncertainty features: 9 for the full-scene case and 6 for the object-centric case. The selections follow three strategies: a) the combination most frequently chosen across all tight brackets with maximum score, b) the combination with the highest overall score, and c) the set of individually most frequently selected uncertainty feature maps. We display the evaluations on all scenes in Tabs. 2 and 3. In both cases we cannot outperform the set of all uncertainty feature maps but also do not sacrifice much performance by any of the selection strategies. This indicates that most of the uncertainty feature maps carry some meaningful information for depth UE.

**Regression Out-of-Scene Generalization** We study our regression models’ generalization to new scenes. Generalization would indicate that the different uncertainty feature maps and their interactions capture error patterns that are at least partially scene-independent. We evaluate each regression model trained on the 13 uncertainty feature maps, with and without direction-dependence. For comparison, we consider the 6 FisherRF-based feature maps. To get more insights into the role of interaction terms and non-

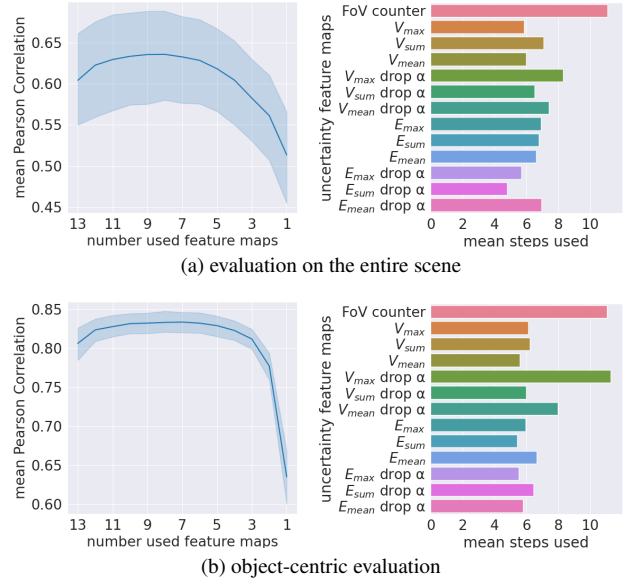


Figure 2. Results of step-wise backward regression to determine the most important uncertainty feature maps. The score on which uncertainty feature maps are dropped is Pearson correlation of the predicted to the true depth error. Investigated where complete scenes (a) and scene limited to the object (b). The plots are the mean score trajectory (left) and the mean number of steps that the uncertainty feature maps were used (right).

linearities, we also consider linear regression. Furthermore, we study the usefulness of training on multiple views from one as well as different scenes to test whether this leads to regression models of stronger generality.

For both rendering and depth UE, on the full scene as well as central objects alone, Tab. 4 presents Pearson correlations averaged over all LF, TUM and combined out-of-scene performances of regressors trained in single-view, multi-view and multi-scene (but one dataset) setups. Overall, our methods clearly outperform (plain) FisherRF even in out-of-scene generalization, despite FisherRF being applied in-scene and outperforming out-of-scene regression-FisherRF. In most cases, gradient boosting trained on direction-dependent features of multiple scenes yields the best out-of-scene UE. However, there are two notable exceptions. First, for full-view rendering UE, linear regression trained on direction-dependent features from single LF views slightly outperforms gradient boosting across all training regimes, including multi-view and multi-scene. Second, for full-view depth UE, TUM single-view linear regression models achieve the highest out-of-scene performance on average. These findings suggest a moderate tendency of gradient boosting to overfit within scenes. Generally, UE generalizes better for depth errors than rendering errors and rather for central objects than full scenes.

views	predicted error type				depth error						rendering error					
	evaluation on dataset scene				entire views			object-centric			entire views			object-centric		
	method	no. of maps	model	training	LF mean	TUM mean	mean	LF mean	TUM mean	mean	LF mean	TUM mean	mean	LF mean	TUM mean	mean
1 view	FisherRF				0.31	-0.08	0.115	0.05	0.303	0.177	-0.224	-0.241	-0.232	0.129	0.458	0.293
	reg. FisherRF	6	grad.	LF	0.24	-0.008	0.116	0.284	0.312	0.298	0.153	0.163	0.158	0.328	0.42	0.374
				TUM	0.139	0.273	0.206	0.245	0.278	0.261	0.104	0.13	0.117	0.273	0.419	0.346
			lin.	LF	0.19	0.123	0.156	0.259	0.253	0.256	0.115	0.078	0.096	0.184	0.386	0.285
				TUM	0.15	0.203	0.177	0.089	0.184	0.137	0.076	0.099	0.087	0.087	0.329	0.208
	vis. err. maps	13	grad.	LF	0.121	0.153	0.137	0.632	0.453	0.543	0.192	0.168	0.18	0.509	0.481	0.495
				TUM	0.187	0.404	0.295	0.514	0.506	0.51	0.122	0.177	0.15	0.398	0.484	0.441
			lin.	LF	0.25	0.097	0.173	0.444	0.128	0.286	0.215	0.197	0.206	0.206	0.013	0.11
				TUM	<b>0.312</b>	0.468	0.39	0.265	0.257	0.261	0.186	0.239	0.213	0.165	0.296	0.23
	vis. err. maps*	13	grad.	LF	0.159	0.104	0.132	0.631	0.452	0.541	0.2	0.167	0.184	0.548	0.506	0.527
				TUM	0.183	0.378	0.281	0.513	0.5	0.507	0.155	0.203	0.179	0.424	0.5	0.462
			lin.	LF	0.242	0.076	0.159	0.384	0.17	0.277	<b>0.288</b>	0.202	0.245	0.179	0.1	0.14
				TUM	0.281	0.413	0.347	0.123	0.166	0.145	0.248	0.259	0.254	0.067	0.262	0.165
m-view	reg. FisherRF	6	grad.	LF	0.243	-0.01	0.117	0.284	0.315	0.299	0.15	0.16	0.155	0.343	0.448	0.395
				TUM	0.193	0.349	0.271	0.31	0.304	0.307	0.145	0.186	0.165	0.308	0.445	0.377
	vis. err. maps	13	grad.	LF	0.13	0.148	0.139	0.657	0.464	0.56	0.194	0.195	0.194	0.491	0.513	0.502
				TUM	0.203	0.477	0.34	0.584	0.577	0.58	0.13	0.226	0.178	0.444	0.5	0.472
	vis. err. maps*	13	grad.	LF	0.153	0.12	0.137	0.644	0.448	0.546	0.206	0.176	0.191	0.551	0.497	0.524
				TUM	0.247	0.45	0.349	0.6	0.585	0.592	0.199	0.257	0.228	0.497	0.524	0.51
	reg. FisherRF	6	grad.	LF	0.083	-0.046	0.019	0.261	0.356	0.309	0.248	0.217	0.232	0.532	0.503	0.517
				TUM	0.201	0.456	0.329	0.419	0.418	0.418	0.213	0.261	0.237	0.434	0.502	0.468
	vis. err. maps	13	grad.	LF	0.039	0.095	0.067	0.687	0.455	0.571	0.264	0.202	0.233	0.575	0.454	0.514
				TUM	0.217	<b>0.561</b>	0.389	0.642	0.628	0.635	0.165	0.305	0.235	0.544	0.559	0.552
	vis. err. maps*	13	grad.	LF	-0.03	-0.004	-0.017	0.663	0.463	0.563	0.266	0.112	0.189	<b>0.611</b>	0.517	0.564
				TUM	0.274	0.545	<b>0.409</b>	<b>0.688</b>	<b>0.645</b>	<b>0.667</b>	0.256	<b>0.333</b>	<b>0.295</b>	0.583	<b>0.572</b>	<b>0.577</b>

Table 4. Pearson Correlation of predicted to true depth/rendering error for entire/object-centric scene evaluation. 1-view, m-view and m-scene describe whether we use one or multiple views of the same or multiple scenes for UE regression (grad. for gradient boosting, lin. for linear regression). All rows except the first are the averages when training the regressor on the dataset in the column ‘training’.

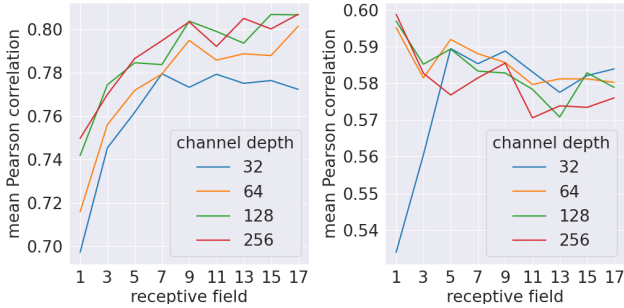


Figure 3. Average in-scene Pearson correlations of predicted and true rendering (left) and depth errors (right) for CNN models with varying receptive field sizes and numbers of uncertainty features.

**The Role of Spatial Interaction** So far, we performed pixel-wise regression on uncertainty feature maps. Here, we study whether incorporating uncertainty features from neighboring pixels improves the estimation of rendering and depth uncertainty which aligns with recent work leveraging spatial context for uncertainty estimation in semantic segmentation via graph neural networks[7]. For this purpose, we replace the pixel-wise gradient boosting regressor with lightweight fully convolutional neural networks (CNNs) and evaluate their UE on the LF dataset. We train 72 CNNs to predict rendering and depth errors on foreground objects, using all 13 direction-independent primitive representations from the first three hold-out views of a scene and testing on the fourth view. Each CNN has a depth

of 4 layers, with kernel sizes in

$$\{(k_1, \dots, k_4) \mid k_i \in \{1, 3, 5\}, k_j + 2 \geq k_i \geq k_j \text{ for } i < j\} \quad (10)$$

and channel depth in  $\{(h, h, h, h) \mid h \in \{32, 64, 128, 256\}\}$ . Notably, CNNs with all kernel sizes set to 1 reduce to pixel-wise fully connected baselines using only  $1 \times 1$  convolutions. As batch size we found 1 most useful and trained all CNNs for 2000 iterations each ranging from  $10^{-3}$  to  $10^{-5}$ , and weight decay of  $10^{-5}$ . UE performances are provided in terms of Pearson correlation between the predicted and true errors, displayed in Fig. 3. Overall, the CNNs did not outperform gradient boosting, which, however, is not the aim of this study. Interestingly, CNNs with larger receptive fields consistently outperform the fully-connected baselines in rendering error estimation, demonstrating the usefulness of neighborhood information for this task. For depth error estimation, increased receptive field size improves performance only for CNNs with 32 channels, which may be attributed to increased model capacity instead of neighborhood information itself.

## 5. Conclusion

In this work, we introduced a generic UE framework for Gaussian splatting. By constructing 3D Gaussian primitive representations of error and visibility, we capture depth and rendering uncertainty. To utilize this information, we render our primitive representations for novel views (resulting in uncertainty feature maps) and aggregate the differ-



ent rendered representations via different single-pixel regression models. In terms of their own AUSE metric, our approach outperforms the existing FisherRF method by up to **75.8** percent points for direction-dependent UE and **78.3** percent points for direction-independent UE. Some uncertainty feature maps constructed by us proved to be very informative for UE, in particular the FoV count. To the best of our knowledge, our regression models are the first UE models that provide out-of-scene generalization. Further studies suggest that additional information can be leveraged from our uncertainty feature maps by considering neighboring pixels in the regression models. We make our code publicly available under [github.com/TBA](https://github.com/TBA).

## Acknowledgment

T.G. and M.R. acknowledge support by the state of North Rhine-Westphalia and the European Union within the EFRE/JTF project “Just scan it 3D”, grant no. EFRE-20800529. E.H. and M.R. acknowledge support through the junior research group project “UnrEAL” by the German Federal Ministry of Education and Research (BMBF), grant no. 01IS22069.

## References

- [1] Luca Savant Aira, Diego Valsesia, and Enrico Magli. Modeling uncertainty for gaussian splatting. *IEEE Transactions on Neural Networks and Learning Systems*, 36(6):11657–11663, 2025. 1, 2, 3
- [2] Niki Amini-Naieni, Tomas Jakab, Andrea Vedaldi, and Ronald Clark. Instant uncertainty calibration of nerfs using a meta-calibrator. In *European Conference on Computer Vision*, pages 309–324. Springer, 2025. 2
- [3] Jonathan T. Barron, Ben Mildenhall, Dor Verbin, Pratul P. Srinivasan, and Peter Hedman. Mip-nerf 360: Unbounded anti-aliased neural radiance fields. In *Proceedings of the IEEE/CVF Conference on Computer Vision and Pattern Recognition (CVPR)*, pages 5470–5479, 2022. 1
- [4] Pascal Colling, Matthias Rottmann, Lutz Roesse-Koerner, and Hanno Gottschalk. Prediction quality meta regression and error meta classification for segmented lidar point clouds. *International Journal on Artificial Intelligence Tools*, 32(05):2360006, 2023. 4
- [5] Nicholas I Fisher, Toby Lewis, and Brian JJ Embleton. *Statistical analysis of spherical data*. Cambridge university press, 1993. 4
- [6] Chenyu Han and Corentin Dumery. View-dependent uncertainty estimation of 3d gaussian splatting. *arXiv preprint arXiv:2504.07370*, 2025. 3
- [7] Edgar Heinert, Stephan Tilgner, Timo Palm, and Matthias Rottmann. Uncertainty and prediction quality estimation for semantic segmentation via graph neural networks. In *Proceedings of the BMVC 2024 Workshop on Robust Recognition in the Open World (RROW)*. British Machine Vision Association, 2024. 4, 8
- [8] Binbin Huang, Zehao Yu, Anpei Chen, Andreas Geiger, and Shenghua Gao. 2d gaussian splatting for geometrically accurate radiance fields. In *ACM SIGGRAPH 2024 conference papers*, pages 1–11, 2024. 1
- [9] Letian Huang, Jiayang Bai, Jie Guo, and Yanwen Guo. Gs++: Error analyzing and optimal gaussian splatting. *arXiv preprint arXiv:2402.00752*, 2(3), 2024. 1
- [10] Eddy Ilg, Ozgun Cicek, Silvio Galesso, Aaron Klein, Osama Makansi, Frank Hutter, and Thomas Brox. Uncertainty estimates and multi-hypotheses networks for optical flow. In *Proceedings of the European Conference on Computer Vision (ECCV)*, pages 652–667, 2018. 5
- [11] Wen Jiang, Boshu Lei, and Kostas Daniilidis. Fisherrf: Active view selection and uncertainty quantification for radiance fields using fisher information. *arXiv*, 2023. 1, 2, 3, 5, 11
- [12] Jaewoo Jung, Jisang Han, Honggyu An, Jiwon Kang, Seonghoon Park, and Seungryong Kim. Relaxing accurate initialization constraint for 3d gaussian splatting. 2024. 1
- [13] James T Kajiya and Brian P Von Herzen. Ray tracing volume densities. *ACM SIGGRAPH computer graphics*, 18(3):165–174, 1984. 1
- [14] Bernhard Kerbl, Georgios Kopanas, Thomas Leimkuehler, and George Drettakis. 3d gaussian splatting for real-time radiance field rendering. *ACM Transactions on Graphics (TOG)*, 42(4):1–14, 2023. 1, 5, 11
- [15] Kamil Kowol, Matthias Rottmann, Stefan Bracke, and Hanno Gottschalk. Yodar: Uncertainty-based sensor fusion for vehicle detection with camera and radar sensors. In *Proceedings of the 13th International Conference on Agents and Artificial Intelligence*, pages 177–186. SCITEPRESS-Science and Technology Publications, 2021. 4
- [16] Jonas Kulhanek, Songyou Peng, Zuzana Kukelova, Marc Pollefeys, and Torsten Sattler. WildGaussians: 3D gaussian splatting in the wild. *NeurIPS*, 2024. 2
- [17] Kehan Long, Cheng Qian, Jorge Cortés, and Nikolay Atanasov. Learning barrier functions with memory for robust safe navigation. *IEEE Robotics and Automation Letters*, 6(3):4931–4938, 2021. 1
- [18] Kira Maag, Matthias Rottmann, Serin Varghese, Fabian Hüger, Peter Schlicht, and Hanno Gottschalk. Improving video instance segmentation by light-weight temporal uncertainty estimates. In *2021 International Joint Conference on Neural Networks (IJCNN)*, pages 1–8. IEEE, 2021. 4
- [19] Kanti V Mardia and Peter E Jupp. *Directional statistics*. John Wiley & Sons, 2009. 4
- [20] Ricardo Martin-Brualla, Noha Radwan, Mehdi SM Sajjadi, Jonathan T Barron, Alexey Dosovitskiy, and Daniel Duckworth. Nerf in the wild: Neural radiance fields for unconstrained photo collections. In *Proceedings of the IEEE/CVF conference on computer vision and pattern recognition*, pages 7210–7219, 2021. 2
- [21] Hidenobu Matsuki, Riku Murai, Paul HJ Kelly, and Andrew J Davison. Gaussian splatting slam. In *Proceedings of the IEEE/CVF Conference on Computer Vision and Pattern Recognition*, pages 18039–18048, 2024. 1

- [22] N. Max. Optical models for direct volume rendering. *IEEE Transactions on Visualization and Computer Graphics*, 1(2): 99–108, 1995. 1
- [23] Ben Mildenhall, Pratul P Srinivasan, Matthew Tancik, Jonathan T Barron, Ravi Ramamoorthi, and Ren Ng. Nerf: Representing scenes as neural radiance fields for view synthesis. *Communications of the ACM*, 65(1):99–106, 2021. 1
- [24] Claus Müller. *Spherical harmonics*. Springer, 2006. 3
- [25] Alexey Natekin and Alois Knoll. Gradient boosting machines, a tutorial. *Frontiers in neurorobotics*, 7:21, 2013. 5
- [26] Matthew A. Price and Jason D. McEwen. Differentiable and accelerated spherical harmonic and wigner transforms. *Journal of Computational Physics*, 510:113109, 2024. 3
- [27] Fabio Remondino, Ali Karami, Ziyang Yan, Gabriele Mazzacca, Simone Rigon, and Rongjun Qin. A critical analysis of nerf-based 3d reconstruction. *Remote Sensing*, 15(14): 3585, 2023. 1
- [28] Matthias Rottmann, Pascal Colling, Thomas Paul Hack, Robin Chan, Fabian Hüger, Peter Schlicht, and Hanno Gottschalk. Prediction error meta classification in semantic segmentation: Detection via aggregated dispersion measures of softmax probabilities. In *2020 International Joint Conference on Neural Networks (IJCNN)*, pages 1–9. IEEE, 2020. 4
- [29] Marius Schubert, Karsten Kahl, and Matthias Rottmann. Metadetector: Uncertainty quantification and prediction quality estimates for object detection. In *2021 International Joint Conference on Neural Networks (IJCNN)*, pages 1–10. IEEE, 2021. 4
- [30] Seunghyeon Seo, Yeonjin Chang, and Nojun Kwak. Flipnerf: Flipped reflection rays for few-shot novel view synthesis. In *Proceedings of the IEEE/CVF International Conference on Computer Vision (ICCV)*, pages 22883–22893, 2023. 2
- [31] Afshar Shamsi, Hamzeh Asgharnezhad, Shirin Shamsi Jokandan, Abbas Khosravi, Parham M Kebria, Darius Nahavandi, Saeid Nahavandi, and Dipti Srinivasan. An uncertainty-aware transfer learning-based framework for covid-19 diagnosis. *IEEE transactions on neural networks and learning systems*, 32(4):1408–1417, 2021. 1
- [32] Jianxiong Shen, Antonio Agudo, Francesc Moreno-Noguer, and Adria Ruiz. Conditional-flow nerf: Accurate 3d modelling with reliable uncertainty quantification. In *European Conference on Computer Vision*, pages 540–557. Springer, 2022. 1, 2, 4
- [33] Noah Snavely, Steven M Seitz, and Richard Szeliski. Photo tourism: exploring photo collections in 3d. In *ACM siggraph 2006 papers*, pages 835–846. Association for Computing Machinery, 2006. 1
- [34] J. Sturm, N. Engelhard, F. Endres, W. Burgard, and D. Cremers. A benchmark for the evaluation of rgb-d slam systems. In *Proc. of the International Conference on Intelligent Robot Systems (IROS)*, 2012. 4
- [35] Niko Stünderhauf, Jad Abou-Chakra, and Dimity Miller. Density-aware nerf ensembles: Quantifying predictive uncertainty in neural radiance fields. In *2023 IEEE International Conference on Robotics and Automation (ICRA)*, pages 9370–9376, 2023. 1, 2
- [36] Sebastian Thrun. Probabilistic robotics. *Communications of the ACM*, 45(3):52–57, 2002. 1
- [37] Peng Wang, Lingjie Liu, Yuan Liu, Christian Theobalt, Taku Komura, and Wenping Wang. Neus: Learning neural implicit surfaces by volume rendering for multi-view reconstruction. *arXiv preprint arXiv:2106.10689*, 2021. 1
- [38] Frederik Warburg, Ethan Weber, Matthew Tancik, Aleksander Holynski, and Angjoo Kanazawa. Nerfbusters: Removing ghostly artifacts from casually captured nerfs. In *Proceedings of the IEEE/CVF International Conference on Computer Vision*, pages 18120–18130, 2023. 1
- [39] Joey Wilson, Marcelino Almeida, Min Sun, Sachit Mahajan, Maani Ghaffari, Parker Ewen, Omid Ghasemalizadeh, Cheng-Hao Kuo, and Arnie Sen. Modeling uncertainty in 3d gaussian splatting through continuous semantic splatting, 2024. 2, 3
- [40] Mingqiao Ye, Martin Danelljan, Fisher Yu, and Lei Ke. Gaussian grouping: Segment and edit anything in 3d scenes. In *ECCV*, 2024. 5
- [41] Kaan Yücer, Alexander Sorkine-Hornung, Oliver Wang, and Olga Sorkine-Hornung. Efficient 3D object segmentation from densely sampled light fields with applications to 3D reconstruction. *ACM Transactions on Graphics*, 35(3), 2016. 4
- [42] Jiawei Zhang, Jiahe Li, Xiaohan Yu, Lei Huang, Lin Gu, Jin Zheng, and Xiao Bai. Cor-gs: sparse-view 3d gaussian splatting via co-regularization. In *European Conference on Computer Vision*, pages 335–352. Springer, 2024. 1
- [43] Yuhang Zhang, Joshua Maraval, Zhengyu Zhang, Nicolas Ramin, Shishun Tian, and Lu Zhang. Evaluating human perception of novel view synthesis: Subjective quality assessment of gaussian splatting and nerf in dynamic scenes. *arXiv preprint arXiv:2501.08072*, 2025. 1
- [44] Matthias Zwicker, Hanspeter Pfister, Jeroen Van Baar, and Markus Gross. Ewa volume splatting. In *Proceedings Visualization, 2001. VIS'01.*, pages 29–538. IEEE, 2001. 1, 3

## A. FisherRF Baseline

FisherRF [11] is based on the Fisher information matrix of a GS w.r.t. the gradient of the rendering function. The diagonal entries of this Fisher information matrix correspond to variances of the Gaussian primitive parameters and therefore are used to estimate their uncertainty. The considered Gaussian primitive uncertainty of FisherRF only uses the sum of the color parameter variances including all spherical harmonic parameters, used to make the color direction-dependent. Using the GS rendering (Eq. (2)), pixel-wise uncertainties are obtained. In addition to standard FisherRF, we consider a modification more comparable to our method. That is, we compute 6 uncertainty feature maps based on the Gaussian parameter variances like in FisherRF but for different Gaussian primitive parameters. The 6 uncertainty feature maps are based on the grouping of parameters of Gaussian primitives in 1) mean, 2) scale, 3) rotation, 4) opacity factor, 5) spherical harmonics color parameters of degree zero and 6) the higher degree spherical harmonics color parameters. This grouping of parameters originates from the original GS implementation [14]. For a Gaussian primitive the parameter groups scale and rotation correspond to its covariance matrix. In this way all Gaussian primitive parameters are represented in one of the 6 uncertainty feature maps. We use those 6 uncertainty feature maps as input for regression models in the same manner as for our uncertainty feature maps obtained by our method. This allows us to compare the quality of the different sets of feature maps for UE by evaluating the pixel-wise predicted errors using our evaluation metrics.

## B. In-Scene Uncertainty Estimation

Here, we provide additional observations to our in-scene uncertainty estimation study in the form of tables with performances on the individual scenes of both the LF and TUM datasets. Additionally, we show our results for the evaluation on just the scene background.

**Entire Scene Evaluation** Tab. 5 shows the UE for depth error in the case of evaluating the regression model on views of the full scenes. Overall, many of the trends observed on the entire datasets also hold for the individual scenes. I.e., regression-FisherRF improves on standard FisherRF and our method typically outperforms regression-FisherRF. For FisherRF on TUM, we see that the Pearson correlation of UE to the true depth error fluctuates around zero for the individual scenes which results in a close to zero average. Although the evaluation of FisherRF with Pearson correlation is not completely fair, due to potential nonlinearities in the relation of the UE and error, we can still conclude that such a variation between  $-0.266$  and  $0.228$  makes it not useful for UE on the TUM dataset. Note that, in the main paper, we

compared our methods with FisherRF in terms of their standard evaluation metric AUSE. Regression-FisherRF, on the other hand, shows that the uncertainty feature maps created with the FisherRF methods hold useful uncertainty information on the TUM dataset and that this information benefits from further processing with regression models. That our method outperforms regression-FisherRF on most scenes, demonstrates the greater utility of our uncertainty feature maps. In addition, we observe that on the TUM dataset and when training on our uncertainty feature maps, the linear regressor beats gradient boosting on some scenes which suggests a certain potential for gradient boosting overfitting to its training data. Furthermore, regression on direction-independent uncertainty feature maps for one view sometimes surpasses the direction-dependent ones on multiple views.

In Tab. 6, which shows the Pearson correlation of estimated and true rendering error, we again observe similar trends for the scenes as for the full datasets. This time, FisherRF UE is negatively correlated to the true rendering error for all scenes. Its absolute even surpasses gradient boosting trained on multiple views of the TUM scene *\*cabinet\**. However, it is still outperformed by linear regression, suggesting that gradient boosting may overfit in this case, and that the relationship between uncertainty features and rendering error is relatively simple for this specific scene split. Overall, it seems that UE for rendering error is more challenging than for depth error. At least, this holds for our approach and the case of entire scene evaluation. One reason for this might be that the rendering error considers for each pixel the mean error over all color channels, which introduces additional complexity and might obscure some relations between the uncertainty feature maps and the error in the color channels.

**Object-Centric Evaluation** Tabs. 7 and 8 depict the Pearson correlations of estimated and true depth and rendering error in the object-centric case. We observe generally higher correlations than in the full-scene case for all methods but standard FisherRF. This indicates that the approach for UE based on regression models trained on uncertainty feature maps works better for the investigation of the central object in the scene than the entire scene. The relation between predicted and true errors involves noticeable nonlinearities as gradient boosting consistently outperforms the linear regression models. The results for standard FisherRF clearly differ to the entire scene evaluation. Here, all Pearson correlations of FisherRF UE to the true depth or rendering errors are positive and we see higher correlations on the TUM dataset. Our uncertainty feature maps outperform the FisherRF-based ones in all but one case, namely depth error UE on the TUM scene *\*cabinet\** using linear regression.

views				dataset scene	LF															TUM
	method	no. of maps	model	africa	basket	statue	torch	mean	plant	teddy	coke	dishes	flower	flower2	metallic	metallic2	cabinet	cabinet2	teddy2	mean
1-view	FisherRF			0.108	0.286	0.525	0.323	0.31	0.043	0.063	-0.266	-0.037	-0.242	-0.319	-0.137	-0.15	0.015	-0.072	0.228	-0.08
	reg. FisherRF	6	grad.	0.554	0.625	0.844	0.711	0.683	0.304	0.183	0.61	0.575	0.468	0.255	0.332	0.296	0.269	0.521	0.314	0.375
			lin.	0.316	0.437	0.657	0.399	0.452	0.055	0.089	0.447	0.548	0.435	0.289	0.338	0.239	0.286	0.475	0.149	0.305
	vis. err. maps	13	grad.	0.647	0.719	0.902	0.666	0.734	0.24	0.329	0.628	0.661	0.571	0.427	0.518	0.462	0.686	0.66	0.716	0.536
			lin.	0.518	0.601	0.747	0.315	0.545	0.316	0.384	0.701	0.657	0.672	0.486	0.514	0.57	0.661	0.658	0.666	0.571
		9a	grad.	0.645	0.712	0.894	0.631	0.721	0.244	0.332	0.624	0.654	0.585	0.427	0.512	0.463	0.677	0.648	0.729	0.536
		9b	grad.	0.633	0.709	0.902	0.621	0.716	0.226	0.307	0.63	0.649	0.557	0.416	0.529	0.473	0.656	0.623	0.712	0.525
		9c	grad.	0.635	0.702	0.903	0.592	0.708	0.236	0.327	0.633	0.654	0.575	0.423	0.521	0.469	0.68	0.655	0.715	0.535
	vis. err. maps*	13	grad.	0.651	0.722	0.906	0.679	0.739	0.23	0.266	0.66	0.651	0.57	0.42	0.397	0.505	0.642	0.535	0.636	0.501
			lin.	0.525	0.589	0.753	0.359	0.557	0.238	0.291	0.631	0.665	0.591	0.479	0.519	0.55	0.632	0.582	0.559	0.521
m-view	reg. FisherRF	6	grad.	0.577	0.671	0.849	0.763	0.715	<b>0.442</b>	0.248	0.69	0.645	0.702	0.389	0.576	0.595	0.26	0.645	0.477	0.515
	vis. err. maps	13	grad.	<b>0.685</b>	<b>0.765</b>	<b>0.919</b>	<b>0.739</b>	<b>0.777</b>	0.351	<b>0.482</b>	<b>0.731</b>	<b>0.718</b>	<b>0.756</b>	<b>0.488</b>	<b>0.699</b>	<b>0.666</b>	<b>0.732</b>	<b>0.778</b>	<b>0.776</b>	<b>0.653</b>
	vis. err. maps*	13	grad.	<b>0.694</b>	<b>0.769</b>	<b>0.921</b>	<b>0.768</b>	<b>0.788</b>	0.379	0.357	0.666	0.681	0.71	<b>0.514</b>	<b>0.7</b>	0.601	0.653	0.692	0.703	0.605

Table 5. Pearson Correlation of predicted to true depth error for entire scene evaluation. 1-view and m-view describe whether we use one or multiple views for UE regression (grad. for gradient boosting, lin. for linear regression).

views				dataset scene model	africa	basket	statue	torch	LF		plant	teddy	coke	dishes	flower	flower2	metallic	metallic2	cabinet	cabinet2	teddy2	TUM mean
	method	no. of maps							mean													
1 view	FisherRF				-0.172	-0.271	-0.16	-0.292	-0.224	-0.212	-0.179	-0.262	-0.311	-0.148	-0.334	-0.211	-0.201	-0.26	-0.365	-0.172	-0.241	
	reg. FisherRF	6	grad.	lin.	0.28	0.342	0.282	0.367	0.318	0.203	0.156	0.189	0.208	0.194	0.236	0.142	0.094	0.11	0.323	0.133	0.181	
					0.151	0.212	0.165	0.201	0.182	0.149	0.069	0.168	0.207	0.187	0.195	0.159	0.045	0.131	0.195	0.064	0.143	
	vis. err. maps	13	grad.	lin.	0.409	0.391	0.432	0.416	0.412	0.251	0.244	0.199	0.27	0.256	0.226	0.195	0.137	0.171	0.317	0.119	0.217	
					0.307	0.295	0.244	0.391	0.309	0.327	0.319	0.271	0.315	0.333	0.283	<b>0.312</b>	0.208	<u>0.275</u>	0.363	0.182	0.29	
		9a	grad.		0.399	0.383	0.429	0.416	0.407	0.253	0.25	0.199	0.269	0.253	0.236	0.212	0.143	0.18	0.316	0.131	0.222	
		9b	grad.		0.408	0.386	0.426	0.412	0.408	0.247	0.248	0.196	0.254	0.258	0.216	0.2	0.138	0.167	0.325	0.127	0.216	
		9c	grad.		0.398	0.384	0.427	0.399	0.402	0.24	0.243	0.197	0.267	0.229	0.225	0.182	0.132	0.173	0.315	0.122	0.211	
	vis. err. maps*	13	grad.	lin.	0.418	0.401	0.445	0.411	0.419	0.276	0.259	0.238	0.28	0.233	0.26	0.2	0.196	0.162	0.322	0.102	0.23	
					0.384	0.305	0.311	0.402	0.35	0.306	0.327	0.274	0.328	0.305	0.324	<u>0.27</u>	<u>0.24</u>	<b>0.289</b>	0.39	0.204	0.296	
m-view	reg. FisherRF	6	grad.		0.321	0.383	0.332	0.373	0.352	0.32	0.234	0.301	0.283	0.282	0.345	0.236	0.163	0.17	0.386	0.218	0.267	
	vis. err. maps	13	grad.		<b>0.451</b>	0.413	0.486	0.437	0.446	<b>0.408</b>	0.337	0.27	0.341	<b>0.369</b>	0.338	0.24	0.196	0.22	<b>0.405</b>	0.198	0.302	
	vis. err. maps*	13	grad.		<b>0.451</b>	<b>0.438</b>	<b>0.502</b>	<b>0.44</b>	<b>0.458</b>	<b>0.368</b>	<b>0.372</b>	<b>0.369</b>	<b>0.375</b>	<b>0.336</b>	<b>0.362</b>	0.254	<b>0.265</b>	0.206	0.389	<b>0.235</b>	<b>0.321</b>	

Table 6. Pearson Correlation of predicted to true rendering error for entire scene evaluation. 1-view and m-view describe whether we use one or multiple views for UE regression (grad. for gradient boosting, lin. for linear regression).

**Scene Background Evaluation** Here, we consider the setting of UE for just the pixels of the background of a view. The results of this experiment are displayed in Tabs. 9 and 10, for depth and rendering error respectively. Overall, we observe very similar results as for the evaluation on the entire scene. This is to be expected as on views with a central object and a background, the background generally dominates in terms of the number of pixels that it occupies. Accordingly, we again see positive and negative correlations of standard FisherRF UE to the depth error and negative correlations to the rendering error. Regression-FisherRF is again outperformed by our method in terms of mean Pearson correlation for predicted to true depth and rendering error.

### C. Regression Out-of-Scene Generalization

In this section, we discuss some additional observations for the across scene generalization study. We also provide extended tables containing the generalization results to the individual scenes of LF and TUM.

**Entire Scene Evaluation** In Tab. 11, for UE of depth error in the full-scene case, we notice significant variation of the regressors’ generalization across scenes. For the LF

dataset, we see that on the scenes \*statue\* and \*torch\* FisherRF outperforms all regression models trained on different scenes. However it is worth mentioning that no regression models trained on LF scenes generalize well, which might be due to some property of the dataset like a smaller number of hold-out views per scene. We also notice that no regression model can generalize to the scene \*torch\*, which is the only outdoor scene we consider. Nevertheless, we can observe that regression models are capable to generalize across scenes especially when they are trained on multiple hold-out views of different TUM scenes. For the case of UE on rendering error in the full-scene setting in Tab. 12, we see less variation across rows, indicating more consistent performance of the different UE methods across data setups. We observe the best generalization for the regression models trained on multiple TUM scenes or when using a linear regressor on TUM scenes, suggesting that gradient boosting may occasionally overfit to in-scene data. Noteworthy, use the 6 FisherRF uncertainty feature maps to train the UE regressors leads to noticeably lower generalization across all scenes.

**Object-Centric Evaluation** The results for the generalization study of the regression models to individual scenes



views	dataset scene			LF															TUM	
	method	no. of maps	model	africa	basket	statue	torch	mean	plant	teddy	coke	dishes	flower	flower2	metallic	metallic2	cabinet	cabinet2	teddy2	mean
1 view	FisherRF			-0.032	0.05	0.003	0.18	0.05	0.097	0.238	0.486	0.565	0.464	0.283	0.547	0.375	0.139	-0.029	0.171	0.303
	reg. FisherRF	6	grad.	0.714	0.752	0.643	0.681	0.698	0.509	0.584	0.657	0.568	0.514	0.496	0.675	0.476	0.583	0.351	0.32	0.521
			lin.	0.391	0.38	0.491	0.33	0.398	0.135	0.347	0.587	0.509	0.527	0.331	0.56	0.268	0.489	0.115	0.132	0.364
	vis. err. maps	13	grad.	0.875	0.876	0.789	0.802	0.835	0.786	0.742	0.802	0.77	0.787	0.612	0.85	0.792	0.748	0.631	0.669	0.745
			lin.	0.731	0.759	0.647	0.69	0.707	0.738	0.552	0.73	0.646	0.65	0.327	0.741	0.775	0.475	0.354	0.456	0.586
		6a	grad.	0.871	0.846	0.793	0.78	0.822	0.764	0.697	0.807	0.777	0.774	0.608	0.848	0.78	0.736	0.623	0.678	0.736
		6b	grad.	0.866	0.86	0.779	0.785	0.822	0.783	0.741	0.794	0.771	0.794	0.612	0.861	0.799	0.746	0.625	0.658	0.744
		6c	grad.	0.873	0.861	0.795	0.799	0.832	0.778	0.737	0.81	0.772	0.792	0.608	0.861	0.798	0.753	0.636	0.656	0.746
	vis. err. maps*	13	grad.	0.856	0.885	0.788	0.796	0.831	0.775	0.688	0.772	0.738	0.758	0.606	0.846	0.733	0.779	0.603	0.597	0.718
			lin.	0.534	0.715	0.582	0.615	0.612	0.603	0.38	0.584	0.48	0.52	0.292	0.637	0.389	0.55	0.193	0.153	0.435
m-view	reg. FisherRF	6	grad.	0.762	0.792	0.769	0.703	0.757	0.68	0.793	0.83	0.758	0.719	0.695	0.846	0.663	0.666	0.515	0.535	0.7
	vis. err. maps	13	grad.	<b>0.891</b>	<b>0.897</b>	<b>0.822</b>	<b>0.824</b>	<b>0.859</b>	<b>0.894</b>	<b>0.909</b>	<b>0.9</b>	<b>0.866</b>	<b>0.894</b>	<b>0.749</b>	<b>0.914</b>	<b>0.859</b>	<b>0.813</b>	<b>0.7</b>	<b>0.836</b>	<b>0.849</b>
	vis. err. maps*	13	grad.	<u>0.883</u>	<u>0.905</u>	<u>0.83</u>	<u>0.816</u>	<u>0.859</u>	<u>0.883</u>	<u>0.86</u>	<u>0.887</u>	<u>0.837</u>	<u>0.883</u>	<u>0.74</u>	<u>0.909</u>	<u>0.85</u>	<u>0.79</u>	<u>0.595</u>	<u>0.836</u>	<u>0.825</u>

Table 7. Pearson Correlation of predicted to true depth error for object-centric evaluation. 1-view and m-view describe whether we use one or multiple views for UE regression (grad. for gradient boosting, lin. for linear regression).

views	dataset scene			LF															TUM	
	method	no. of maps	model	africa	basket	statue	torch	mean	plant	teddy	coke	dishes	flower	flower2	metallic	metallic2	cabinet	cabinet2	teddy2	mean
1-view	FisherRF			0.164	0.096	-0.038	0.295	0.129	0.361	0.354	0.713	0.772	0.584	0.347	0.667	0.704	0.212	0.022	0.299	0.458
	reg. FisherRF	6	grad.	0.85	0.595	0.632	0.74	0.704	0.56	0.451	0.874	0.888	0.758	0.517	0.809	0.809	0.641	0.393	0.398	0.645
			lin.	0.687	0.154	0.373	0.4	0.404	0.412	0.293	0.795	0.788	0.803	0.409	0.634	0.744	0.637	0.071	0.168	0.523
	vis. err. maps	13	grad.	0.906	0.706	0.84	0.833	0.822	0.694	0.562	0.932	0.954	0.886	0.607	0.923	0.915	0.736	0.538	0.565	0.756
			lin.	0.765	0.483	0.587	0.698	0.633	0.504	0.448	0.884	0.895	0.797	0.318	0.872	0.895	0.416	0.367	0.392	0.617
		6a	grad.	0.895	0.692	0.833	0.809	0.807	0.668	0.532	0.922	0.953	0.881	0.6	0.916	0.91	0.719	0.551	0.568	0.747
		6b	grad.	0.875	0.679	0.832	0.814	0.8	0.677	0.559	0.93	0.949	0.863	0.598	0.913	0.909	0.72	0.537	0.593	0.75
		6c	grad.	0.895	0.688	0.838	0.824	0.811	0.691	0.542	0.932	0.95	0.858	0.602	0.914	0.907	0.729	0.551	0.572	0.75
	vis. err. maps*	13	grad.	0.895	0.703	0.838	0.837	0.818	0.588	0.544	0.888	0.928	0.856	0.589	0.884	0.885	0.706	0.547	0.549	0.724
			lin.	0.624	0.411	0.517	0.553	0.526	0.312	0.31	0.813	0.814	0.696	0.31	0.802	0.805	0.42	0.271	0.236	0.526
m-view	reg. FisherRF	6	grad.	0.872	0.617	0.769	0.747	0.751	0.748	0.694	0.92	0.913	0.903	0.726	0.864	0.893	0.728	0.488	0.549	0.766
	vis. err. maps	13	grad.	<b>0.914</b>	<b>0.741</b>	<b>0.869</b>	<b>0.846</b>	<b>0.842</b>	<b>0.851</b>	<b>0.773</b>	<b>0.965</b>	<b>0.969</b>	<b>0.942</b>	<b>0.787</b>	<b>0.943</b>	<b>0.951</b>	<b>0.816</b>	<b>0.643</b>	<b>0.717</b>	<b>0.851</b>
	vis. err. maps*	13	grad.	0.904	<b>0.743</b>	<b>0.867</b>	<b>0.853</b>	<b>0.842</b>	0.799	0.747	0.931	0.957	0.917	0.749	0.903	0.931	0.754	0.535	0.697	0.811

Table 8. Pearson Correlation of predicted to true rendering error object-centric evaluation. 1-view and m-view describe whether we use one or multiple views for UE regression (grad. for gradient boosting, lin. for linear regression).

in the object-centric case are provided in Tabs. 13 and 14. In the object-centric case we had higher Person correlations between the predicted and true depth and rendering errors than in the in-scene case. This is also the case in the out-of-scene generalization study. Overall, gradient boosting beats linear regression, multi-view beats single-view and multi-scene beats multi-view, which is not very surprising. Notably, gradient boosting regressors trained on multiple scenes achieve moderate to high correlations between predicted and true error for most scenes.

## D. Visual Uncertainty Estimation Examples

In Figs. 4 and 5, we provide some qualitative examples of the predicted depth and rendering errors for different regression training setups.

views	method	no. of maps	dataset scene model	africa	basket	statue	torch	LF mean	plant	teddy	coke	dishes	flower	flower2	metallic	metallic2	cabinet	cabinet2	teddy2	TUM mean
1 view	FisherRF			0.067	0.099	0.466	0.292	0.231	0.027	0.038	-0.293	-0.115	-0.372	-0.417	-0.155	-0.175	-0.189	-0.189	-0.022	-0.169
	reg. FisherRF	6	grad. lin.	0.541	0.44	0.824	0.704	0.627	0.251	0.109	0.607	0.557	0.582	0.28	0.336	0.301	0.317	0.364	0.22	0.357
	vis. err. maps	13	grad. lin.	0.293	0.147	0.624	0.39	0.363	0.057	0.048	0.448	0.544	0.483	0.311	0.338	0.231	0.237	0.352	0.064	0.283
	vis. err. maps*	13	grad. lin.	0.66	0.59	0.884	0.653	0.697	0.162	0.256	0.643	0.647	0.647	0.425	0.528	0.447	0.683	0.483	0.544	0.497
m-view	reg. FisherRF	6	grad. lin.	0.512	0.332	0.732	0.332	0.477	0.134	0.194	0.647	0.636	0.61	0.405	0.416	0.502	0.634	0.311	0.385	0.443
	vis. err. maps	13	grad. lin.	0.512	0.332	0.732	0.332	0.477	0.133	0.183	0.628	0.649	0.604	0.455	0.514	0.546	0.606	0.29	0.408	0.456
	reg. FisherRF	6	grad. lin.	0.568	0.508	0.835	0.757	0.667	<b>0.416</b>	0.126	0.692	0.624	<b>0.748</b>	0.417	0.577	0.607	0.4	0.483	0.424	0.501
	vis. err. maps*	13	grad. lin.	0.692	<b>0.653</b>	0.905	0.73	0.745	0.307	<b>0.389</b>	<b>0.731</b>	<b>0.696</b>	0.738	0.467	0.687	<b>0.641</b>	<b>0.782</b>	<b>0.631</b>	<b>0.653</b>	<b>0.611</b>
				<b>0.693</b>	<b>0.649</b>	<b>0.913</b>	<b>0.758</b>	<b>0.753</b>	0.334	0.241	0.669	<b>0.663</b>	0.719	<b>0.519</b>	<b>0.706</b>	0.59	<b>0.717</b>	<b>0.539</b>	<b>0.568</b>	<b>0.57</b>

Table 9. Pearson Correlation of predicted to true depth error for scene background evaluation. 1-view and m-view describe whether we use one or multiple views for UE regression (grad. for gradient boosting, lin. for linear regression).

views	method	no. of maps	dataset scene model	africa	basket	statue	torch	LF mean	plant	teddy	coke	dishes	flower	flower2	metallic	metallic2	cabinet	cabinet2	teddy2	TUM mean
1 view	FisherRF			-0.187	-0.295	-0.248	-0.33	-0.265	-0.227	-0.183	-0.255	-0.342	-0.162	-0.347	-0.212	-0.2	-0.258	-0.373	-0.25	-0.255
	reg. FisherRF	6	grad. lin.	0.304	0.355	0.28	0.383	0.33	0.181	0.147	0.183	0.228	0.213	0.248	0.146	0.093	0.11	0.305	0.153	0.183
	vis. err. maps	13	grad. lin.	0.156	0.241	0.174	0.218	0.198	0.155	0.074	0.164	0.203	0.19	0.191	0.158	0.041	0.089	0.203	0.106	0.143
	vis. err. maps*	13	grad. lin.	0.412	0.415	0.412	0.403	0.41	0.223	0.243	0.199	0.256	0.24	0.216	0.179	0.139	0.11	0.283	0.105	0.199
m-view	reg. FisherRF	6	grad. lin.	0.306	0.409	0.222	0.402	0.335	0.305	0.32	0.268	0.325	0.343	0.286	<b>0.312</b>	0.207	<b>0.2</b>	0.338	0.166	0.279
	vis. err. maps	13	grad. lin.	0.419	0.424	0.431	0.406	0.42	0.251	0.255	0.239	0.276	0.222	0.245	0.202	0.204	0.114	0.293	0.112	0.219
	vis. err. maps*	13	grad. lin.	0.385	0.404	0.308	0.41	0.377	0.301	0.327	0.279	0.316	0.298	0.305	0.271	0.234	<b>0.225</b>	0.366	0.174	0.282
	reg. FisherRF	6	grad. lin.	0.343	0.393	0.329	0.395	0.365	0.323	0.234	<b>0.3</b>	0.293	0.318	<b>0.367</b>	0.232	0.16	0.178	<b>0.388</b>	<b>0.233</b>	0.275
m-view	vis. err. maps	13	grad. lin.	0.448	0.459	0.463	<b>0.431</b>	0.45	<b>0.406</b>	0.34	0.275	0.34	<b>0.351</b>	0.342	0.256	0.205	0.14	0.369	0.199	0.293
	vis. err. maps*	13	grad. lin.	<b>0.456</b>	<b>0.468</b>	<b>0.492</b>	0.429	<b>0.461</b>	0.358	<b>0.368</b>	<b>0.371</b>	<b>0.385</b>	0.321	0.36	0.247	<b>0.282</b>	0.119	<b>0.398</b>	0.221	<b>0.312</b>

Table 10. Pearson Correlation of predicted to true rendering error for scene background evaluation. 1-view and m-view describe whether we use one or multiple views for UE regression (grad. for gradient boosting, lin. for linear regression).

views	method	no. of maps	dataset scene model	training	africa	basket	statue	torch	LF mean	plant	teddy	coke	dishes	flower	flower2	metallic	metallic2	cabinet	cabinet2	teddy2	TUM mean
1 view	FisherRF				0.108	0.286	<b>0.525</b>	<b>0.323</b>	0.31	0.043	0.063	-0.266	-0.037	-0.242	-0.319	-0.137	-0.15	0.015	-0.072	0.228	-0.08
	reg. FisherRF	6	grad. LF		0.196	0.238	0.301	0.226	0.14	0.088	0.069	-0.165	-0.038	-0.118	-0.15	-0.036	-0.093	0.106	0.034	0.216	-0.008
			lin. TUM		0.156	0.23	0.186	-0.016	0.239	0.189	0.15	0.444	0.405	0.21	0.337	0.299	0.273	0.157	0.313	0.229	0.273
			lin. TUM		0.099	0.202	0.299	0.158	0.19	0.089	0.086	0.146	0.215	0.085	0.068	0.173	0.069	0.099	0.169	0.15	0.123
			lin. TUM		0.103	0.189	0.344	-0.035	0.15	0.15	0.071	0.321	0.385	0.203	0.211	0.252	0.202	0.104	0.221	0.115	0.203
	vis. err. maps	13	grad. LF		0.05	0.227	0.235	-0.026	0.121	0.095	0.016	0.174	0.261	0.141	0.189	0.089	0.148	0.167	0.176	0.222	0.153
			lin. TUM		0.171	0.27	0.256	0.049	0.187	0.213	0.245	0.496	0.471	0.32	0.502	0.389	0.45	0.404	0.44	0.514	0.404
			lin. TUM		<b>0.357</b>	0.42	0.225	-0.002	0.25	0.111	0.062	0.139	0.198	0.08	0.127	0.071	0.077	0.027	0.061	0.108	0.097
			lin. TUM		0.338	<b>0.495</b>	0.338	0.077	<b>0.312</b>	0.309	0.34	0.606	0.569	<b>0.436</b>	0.504	0.394	0.447	0.445	0.513	0.588	0.468
	vis. err. maps*	13	grad. LF		0.058	0.251	0.286	0.043	0.159	0.028	-0.048	0.036	0.146	0.139	0.213	0.007	0.046	0.209	0.201	0.17	0.104
			lin. TUM		0.164	0.256	0.265	0.047	0.183	0.194	0.189	0.483	0.473	0.31	0.482	0.384	0.427	0.374	0.395	0.451	0.378
			lin. TUM		0.311	0.413	0.236	0.009	0.242	0.049	0.005	0.064	0.178	0.173	0.13	-0.021	-0.021	0.078	0.116	0.085	0.076
m-view	reg. FisherRF	6	grad. LF		0.208	0.244	0.298	0.222	0.243	0.106	0.069	-0.172	-0.043	-0.125	-0.146	-0.026	-0.089	0.079	0.019	0.221	-0.01
			lin. TUM		0.259	0.292	0.224	-0.002	0.193	0.245	0.2	0.533	0.503	0.27	0.41	0.387	0.325	0.207	0.414	0.34	0.349
	vis. err. maps	13	grad. LF		0.063	0.247	0.232	-0.022	0.13	0.093	-0.013	0.206	0.256	0.157	0.177	0.116	0.148	0.122	0.169	0.201	0.148
			lin. TUM		0.157	0.283	0.311	0.06	0.203	0.28	0.34	0.589	0.558	0.376	0.588	0.494	0.54	0.426	0.461	0.6	0.477
	vis. err. maps*	13	grad. LF		0.075	0.262	0.217	0.058	0.153	0.054	-0.039	0.037	0.192	0.171	0.23	-0.009	0.052	0.22	0.225	0.187	0.12
			lin. TUM		0.221	0.348	0.338	0.08	0.247	0.254	0.266	0.563	0.567	0.355	0.56	0.465	0.5	0.438	0.445	0.541	0.45
	reg. FisherRF	6	grad. LF		0.153	-	-	0.014	0.083	0.055	0.039	-0.213	-0.01	-0.03	-0.227	-0.099	-0.191	0.029	-0.038	0.176	-0.046
			lin. TUM		0.301	0.41	0.203	-0.108	0.201	0.312	0.281	0.689	<b>0.697</b>	0.319	0.553	0.53	<b>0.581</b>	0.189	0.458	0.403	0.456
	vis. err. maps	13	grad. LF		0.132	-	-	-0.054	0.039	0.113	0.026	0.092	0.242	0.09	0.123	-0.005	0.099	0.033	0.102	0.133	0.095
			lin. TUM		0.078	0.165	0.56	0.064	0.217	<b>0.332</b>	<b>0.441</b>	<b>0.721</b>	0.631	0.381	<b>0.687</b>	<b>0.571</b>	<b>0.606</b>	<b>0.553</b>	<b>0.569</b>	<b>0.682</b>	<b>0.561</b>
	vis. err. maps*	13	grad. LF		0.107	-	-	-0.167	-0.03	0.051	-0.011	-0.083	0.051	0.024	0.009	-0.11	-0.057	0.019	0.012	0.046	-0.004
			lin. TUM		0.214	0.301	0.495	0.085	0.274	0.303	0.394	0.7	<b>0.689</b>	0.421	0.669	0.542	0.559	<b>0.563</b>	0.565	0.589	0.545

Table 11. Pearson Correlation of predicted to true depth error for entire scene evaluation. 1-view, m-view and m-scene describe whether we use one or multiple views of the same or multiple scenes for UE regression (grad. for gradient boosting, lin. for linear regression). All rows except the first are the averages when training the regressor on the dataset in the column 'training'.

views	method	no. of maps	model	dataset scene training					LF												TUM
					africa	basket	statue	torch	mean	plant	teddy	coke	dishes	flower	flower2	metallic	metallic2	cabinet	cabinet2	teddy2	mean
1 view	FisherRF	6	grad.	LF	-0.172	-0.271	-0.16	-0.292	-0.224	-0.212	-0.179	-0.262	-0.311	-0.148	-0.334	-0.211	-0.201	-0.26	-0.365	-0.172	-0.241
	reg. FisherRF			TUM	0.142	0.168	0.125	0.177	0.153	0.119	0.101	0.174	0.196	0.228	0.151	0.141	0.154	0.116	0.27	0.148	0.163
			lin.	LF	0.084	0.117	0.064	0.15	0.104	0.085	0.092	0.155	0.146	0.158	0.133	0.123	0.12	0.093	0.211	0.114	0.13
				TUM	0.093	0.175	0.144	0.046	0.115	-0.072	0.036	0.087	0.143	0.133	0.077	0.055	0.079	0.121	0.122	0.082	0.078
	vis. err. maps	13	grad.	LF	0.049	0.086	0.105	0.062	0.076	0.013	0.038	0.112	0.172	0.152	0.089	0.085	0.07	0.135	0.142	0.087	0.099
				TUM	0.159	0.19	0.187	0.232	0.192	0.185	0.186	0.201	0.196	0.097	0.226	0.192	0.183	0.103	0.187	0.09	0.168
			lin.	LF	0.117	0.106	0.078	0.188	0.122	0.19	0.2	0.202	0.214	0.134	0.213	0.191	0.182	0.103	0.204	0.112	0.177
				TUM	0.228	0.173	0.173	0.286	0.215	0.237	0.25	0.22	0.313	0.182	0.133	0.151	0.155	0.15	0.249	0.128	0.197
	vis. err. maps*	13	grad.	LF	0.205	0.118	0.131	0.292	0.186	0.293	0.287	0.276	0.304	0.236	0.234	0.199	0.211	0.149	0.277	0.161	0.239
				TUM	0.192	0.194	0.179	0.237	0.2	0.179	0.203	0.153	0.208	0.122	0.203	0.172	0.225	0.121	0.214	0.037	0.167
			lin.	LF	0.149	0.133	0.119	0.22	0.155	0.205	0.21	0.222	0.239	0.222	0.218	0.202	0.213	0.143	0.24	0.119	0.203
				TUM	<b>0.342</b>	<b>0.247</b>	0.198	<b>0.367</b>	<b>0.288</b>	0.326	0.312	0.176	0.278	0.214	0.151	0.154	0.162	0.107	0.23	0.115	0.202
m-view	reg. FisherRF	6	grad.	LF	<b>0.299</b>	0.172	0.19	0.333	0.248	<b>0.334</b>	0.318	0.275	0.315	0.299	0.253	0.235	0.247	0.139	0.279	0.152	0.259
				TUM	0.157	0.188	0.11	0.143	0.15	0.125	0.096	0.174	0.197	0.229	0.154	0.13	0.147	0.114	0.25	0.146	0.16
	vis. err. maps		grad.	LF	0.129	0.161	0.091	0.2	0.145	0.138	0.133	0.223	0.221	0.239	0.185	0.171	0.145	0.144	0.282	0.165	0.186
				TUM	0.169	0.187	0.183	0.236	0.194	0.214	0.219	0.235	0.232	0.111	0.27	0.21	0.225	0.121	0.207	0.102	0.195
	vis. err. maps*	13	grad.	LF	0.12	0.107	0.057	0.236	0.13	0.251	0.258	0.259	0.27	0.181	0.268	0.247	0.234	0.126	0.252	0.142	0.226
				TUM	0.197	0.183	0.204	0.24	0.206	0.181	0.222	0.158	0.211	0.143	0.216	0.194	0.222	0.117	0.237	0.034	0.176
			lin.	LF	0.204	0.15	0.144	0.297	0.199	0.253	0.27	0.289	0.304	0.292	0.265	0.25	0.264	0.183	0.305	0.15	0.257
				TUM	0.244	-	-	0.252	0.248	0.201	0.141	0.241	0.25	0.295	0.19	0.196	0.202	0.132	0.322	0.21	0.217
	vis. err. maps	13	grad.	LF	0.189	0.228	0.142	0.292	0.213	0.224	0.162	0.32	0.308	0.33	0.244	0.259	0.193	0.21	<b>0.384</b>	<b>0.238</b>	0.261
				TUM	0.259	-	-	0.268	0.264	0.213	0.214	0.24	0.246	0.136	0.292	0.214	0.218	0.127	0.231	0.094	0.202
			lin.	LF	0.161	0.122	0.06	0.319	0.165	0.327	<b>0.347</b>	<b>0.334</b>	<b>0.342</b>	0.274	<b>0.348</b>	<b>0.337</b>	<b>0.28</b>	<b>0.21</b>	0.37	0.187	0.305
				TUM	0.277	-	-	0.254	0.266	0.13	0.18	0.011	0.113	0.041	0.161	0.101	0.138	0.125	0.228	0.009	0.112
m-scene	vis. err. maps*	13	grad.	LF	0.279	0.21	0.158	<b>0.379</b>	0.256	0.298	<b>0.355</b>	<b>0.356</b>	<b>0.379</b>	<b>0.386</b>	0.336	0.316	<b>0.331</b>	<b>0.271</b>	<b>0.405</b>	0.233	<b>0.333</b>
				TUM																	
			lin.	LF																	
				TUM																	

Table 12. Pearson Correlation of predicted to true rendering error for entire scene evaluation. 1-view, m-view and m-scene describe whether we use one or multiple views of the same or multiple scenes for UE regression (grad. for gradient boosting, lin. for linear regression). All rows except the first are the averages when training the regressor on the dataset in the column 'training'.

views					dataset scene					LF												TUM
	method	no. of maps	model	training	africa	basket	statue	torch	mean	plant	teddy	coke	dishes	flower	flower2	metallic	metallic2	cabinet	cabinet2	teddy2	mean	
1 view	FisherRF				-0.032	0.05	0.003	0.18	0.05	0.097	0.238	0.486	0.565	0.464	0.283	0.547	0.375	0.139	-0.029	0.171	0.303	
	reg. FisherRF	6	grad.	LF	0.196	0.355	0.242	0.344	0.284	0.329	0.398	0.435	0.369	0.346	0.387	0.343	0.335	0.196	0.038	0.254	0.312	
				TUM	0.209	0.29	0.217	0.264	0.245	0.259	0.327	0.402	0.312	0.286	0.324	0.341	0.347	0.183	0.065	0.207	0.278	
			lin.	LF	0.139	0.27	0.398	0.231	0.259	0.153	0.314	0.457	0.384	0.148	0.245	0.399	0.343	0.355	-0.085	0.067	0.253	
				TUM	0.084	0.062	0.117	0.094	0.089	0.082	0.179	0.387	0.351	0.075	0.143	0.328	0.293	0.188	-0.054	0.051	0.184	
	vis. err. maps	13	grad.	LF	0.599	0.697	0.617	0.616	0.632	0.532	0.479	0.547	0.497	0.414	0.565	0.499	0.54	0.303	0.221	0.39	0.453	
				TUM	0.522	0.596	0.407	0.532	0.514	0.56	0.473	0.658	0.562	0.471	0.607	0.62	0.616	0.364	0.238	0.396	0.506	
			lin.	LF	0.458	0.521	0.236	0.56	0.444	0.397	0.213	0.278	-0.036	0.168	0.107	-0.028	0.16	-0.024	0.098	0.075	0.128	
				TUM	0.207	0.298	0.214	0.339	0.265	0.401	0.295	0.402	0.353	0.102	0.224	0.357	0.426	-0.025	0.061	0.231	0.257	
	vis. err. maps*	13	grad.	LF	0.613	0.695	0.613	0.604	0.631	0.551	0.48	0.564	0.471	0.391	0.547	0.486	0.549	0.296	0.23	0.404	0.452	
				TUM	0.512	0.586	0.426	0.528	0.513	0.517	0.439	0.665	0.544	0.487	0.609	0.603	0.619	0.391	0.26	0.369	0.5	
			lin.	LF	0.338	0.442	0.309	0.445	0.384	0.428	0.233	0.192	0.21	0.101	0.233	0.174	0.311	-0.11	-0.037	0.136	0.17	
			TUM	0.17	0.125	0.046	0.152	0.123	0.162	0.179	0.312	0.264	0.104	0.236	0.226	0.262	0.029	-0.017	0.07	0.166		
m-view	reg. FisherRF	6	grad.	LF	0.172	0.36	0.263	0.34	0.284	0.333	0.405	0.435	0.396	0.36	0.394	0.362	0.348	0.175	0.005	0.253	0.315	
				TUM	0.239	0.387	0.303	0.31	0.31	0.333	0.391	0.407	0.339	0.305	0.323	0.298	0.359	0.183	0.113	0.287	0.304	
	vis. err. maps	13	grad.	LF	0.627	0.714	0.635	0.65	0.657	0.564	0.483	0.553	0.493	0.451	0.556	0.488	0.56	0.32	0.244	0.392	0.464	
				TUM	0.556	0.685	0.485	0.608	0.584	0.696	0.595	0.726	0.595	0.523	0.66	0.64	0.699	0.378	0.309	0.528	0.577	
	vis. err. maps*	13	grad.	LF	0.616	0.695	0.639	0.624	0.644	0.584	0.501	0.532	0.453	0.41	0.538	0.447	0.532	0.28	0.237	0.413	0.448	
				TUM	0.576	0.681	0.541	0.601	0.6	0.661	0.559	0.744	0.635	0.55	0.696	0.672	0.725	<b>0.417</b>	0.277	0.495	0.585	
m-scene	reg. FisherRF	6	grad.	LF	0.154	-	-	0.369	0.261	0.35	0.507	0.521	0.391	0.377	0.406	0.463	0.398	0.167	0.031	0.305	0.356	
				TUM	0.384	0.509	0.431	0.351	0.419	0.386	0.482	0.679	0.369	0.402	0.415	0.572	0.564	0.265	0.03	0.43	0.418	
	vis. err. maps	13	grad.	LF	<b>0.734</b>	-	-	0.64	<b>0.687</b>	0.66	0.457	0.451	0.418	0.43	0.526	0.353	0.52	0.343	<b>0.376</b>	0.47	0.455	
				TUM	0.592	0.707	0.583	<b>0.683</b>	0.642	<b>0.779</b>	<b>0.68</b>	<b>0.825</b>	0.621	<b>0.575</b>	<b>0.701</b>	<b>0.844</b>	<b>0.831</b>	0.335	0.125	<b>0.593</b>	<b>0.628</b>	
	vis. err. maps*	13	grad.	LF	<b>0.697</b>	-	-	0.629	0.663	0.653	0.486	0.489	0.414	0.411	0.507	0.392	0.537	0.355	<b>0.361</b>	0.483	0.463	
				TUM	0.647	0.772	0.64	<b>0.695</b>	<b>0.688</b>	<b>0.761</b>	<b>0.657</b>	<b>0.836</b>	<b>0.671</b>	<b>0.588</b>	<b>0.777</b>	0.843	<b>0.849</b>	0.361	0.149	<b>0.606</b>	<b>0.645</b>	

views	method	no. of maps	model	dataset scene	africa	basket	statue	torch	LF mean	plant	teddy	coke	dishes	flower	flower2	metallic	metallic2	cabinet	cabinet2	teddy2	TUM mean
				training																	
1 view	FisherRF				0.164	0.096	-0.038	0.295	0.129	0.361	0.354	0.713	<b>0.772</b>	0.584	0.347	0.667	0.704	0.212	0.022	0.299	0.458
	reg. FisherRF	6	grad.	LF	0.379	0.222	0.257	0.454	0.328	0.425	0.366	0.665	0.565	0.394	0.529	0.517	0.576	0.228	0.051	0.304	0.42
				TUM	0.382	0.212	0.165	0.332	0.273	0.4	0.331	0.65	0.57	0.402	0.496	0.555	0.621	0.258	0.057	0.265	0.419
			lin.	LF	0.245	0.036	0.177	0.277	0.184	0.39	0.296	0.722	0.685	0.267	0.269	0.496	0.67	0.423	-0.092	0.123	0.386
				TUM	0.263	0.003	-0.038	0.122	0.087	0.341	0.209	0.639	0.574	0.254	0.219	0.451	0.56	0.279	-0.02	0.108	0.329
	vis. err. maps	13	grad.	LF	0.557	0.424	0.595	0.461	0.509	0.412	0.398	0.653	0.546	0.46	0.563	0.561	0.595	0.378	0.314	0.413	0.481
				TUM	0.545	0.283	0.275	0.488	0.398	0.389	0.34	0.723	0.63	0.48	0.636	0.654	0.676	0.293	0.183	0.318	0.484
			lin.	LF	0.217	0.183	0.056	0.37	0.206	0.185	0.231	0.002	-0.274	0.157	0.007	-0.145	-0.117	-0.062	0.097	0.062	0.013
				TUM	0.282	0.104	0.038	0.236	0.165	0.303	0.27	0.503	0.473	0.21	0.219	0.426	0.505	0.082	0.035	0.225	0.296
	vis. err. maps*	13	grad.	LF	0.536	<u>0.464</u>	<b>0.665</b>	0.526	0.548	0.414	0.409	0.671	0.591	0.453	0.606	0.637	0.671	0.398	0.298	0.418	0.506
				TUM	0.574	0.294	0.35	0.475	0.424	0.36	0.339	0.758	0.619	0.504	0.651	0.68	0.708	0.348	0.221	0.307	0.5
			lin.	LF	0.162	0.121	0.163	0.27	0.179	0.268	0.265	-0.021	0.13	0.147	0.128	0.039	0.097	-0.032	-0.042	0.122	0.1
				TUM	0.283	0.009	-0.068	0.045	0.067	0.11	0.165	0.502	0.453	0.246	0.341	0.408	0.511	0.063	-0.008	0.095	0.262
m-view	reg. FisherRF	6	grad.	LF	0.388	0.234	0.268	0.48	0.343	0.467	0.385	0.67	0.644	0.402	0.561	0.585	0.637	0.269	-0.007	0.31	0.448
				TUM	0.391	0.249	0.223	0.37	0.308	0.425	0.348	0.684	0.612	0.454	0.519	0.582	0.653	0.286	0.052	0.282	0.445
	vis. err. maps	13	grad.	LF	0.538	0.394	0.585	0.448	0.491	0.446	0.403	0.698	0.599	0.465	0.586	0.629	0.642	0.405	0.347	0.424	0.513
				TUM	0.566	0.318	0.339	0.554	0.444	0.435	0.367	0.736	0.6	0.535	0.645	0.637	0.68	0.299	0.214	0.349	0.5
	vis. err. maps*	13	grad.	LF	0.517	<b>0.472</b>	0.685	0.528	0.551	0.415	0.42	0.651	0.561	0.437	0.556	0.637	0.667	0.389	0.314	0.42	0.497
				TUM	0.598	0.357	0.473	0.561	0.497	0.404	0.369	0.773	0.647	0.564	0.688	0.692	0.719	0.349	0.225	0.331	0.524
m-scene	reg. FisherRF	6	grad.	LF	0.526	-	-	0.538	0.532	0.491	0.436	0.794	0.672	0.441	0.599	0.679	0.69	0.304	0.078	0.344	0.503
				TUM	0.562	0.316	0.413	0.445	0.434	0.507	0.48	0.792	0.569	0.499	0.52	0.777	0.815	0.265	-0.067	0.369	0.502
	vis. err. maps	13	grad.	LF	0.565	-	-	0.585	0.575	0.522	0.492	0.509	0.3	0.512	0.475	0.316	0.374	<u>0.5</u>	<b>0.431</b>	<b>0.563</b>	0.454
				TUM	<u>0.646</u>	0.4	0.483	<b>0.648</b>	0.544	<b>0.598</b>	0.496	<b>0.881</b>	0.728	<u>0.595</u>	0.64	<u>0.858</u>	<b>0.906</b>	0.198	-0.025	0.277	<u>0.559</u>
	vis. err. maps*	13	grad.	LF	0.612	-	-	0.609	<b>0.611</b>	0.445	<b>0.534</b>	0.635	0.475	0.514	0.531	0.53	0.602	<b>0.541</b>	0.383	0.498	0.517
				TUM	<b>0.654</b>	0.44	0.598	0.64	0.583	0.525	0.498	0.879	0.753	<b>0.6</b>	<b>0.753</b>	<b>0.861</b>	0.893	0.234	-0.003	0.295	<b>0.572</b>

Table 14. Pearson Correlation of predicted to true rendering error for object-centric evaluation. 1-view, m-view and m-scene describe whether we use one or multiple views of the same or multiple scenes for UE regression (grad. for gradient boosting, lin. for linear regression). All rows except the first are the averages when training the regressor on the dataset in the column 'training'.



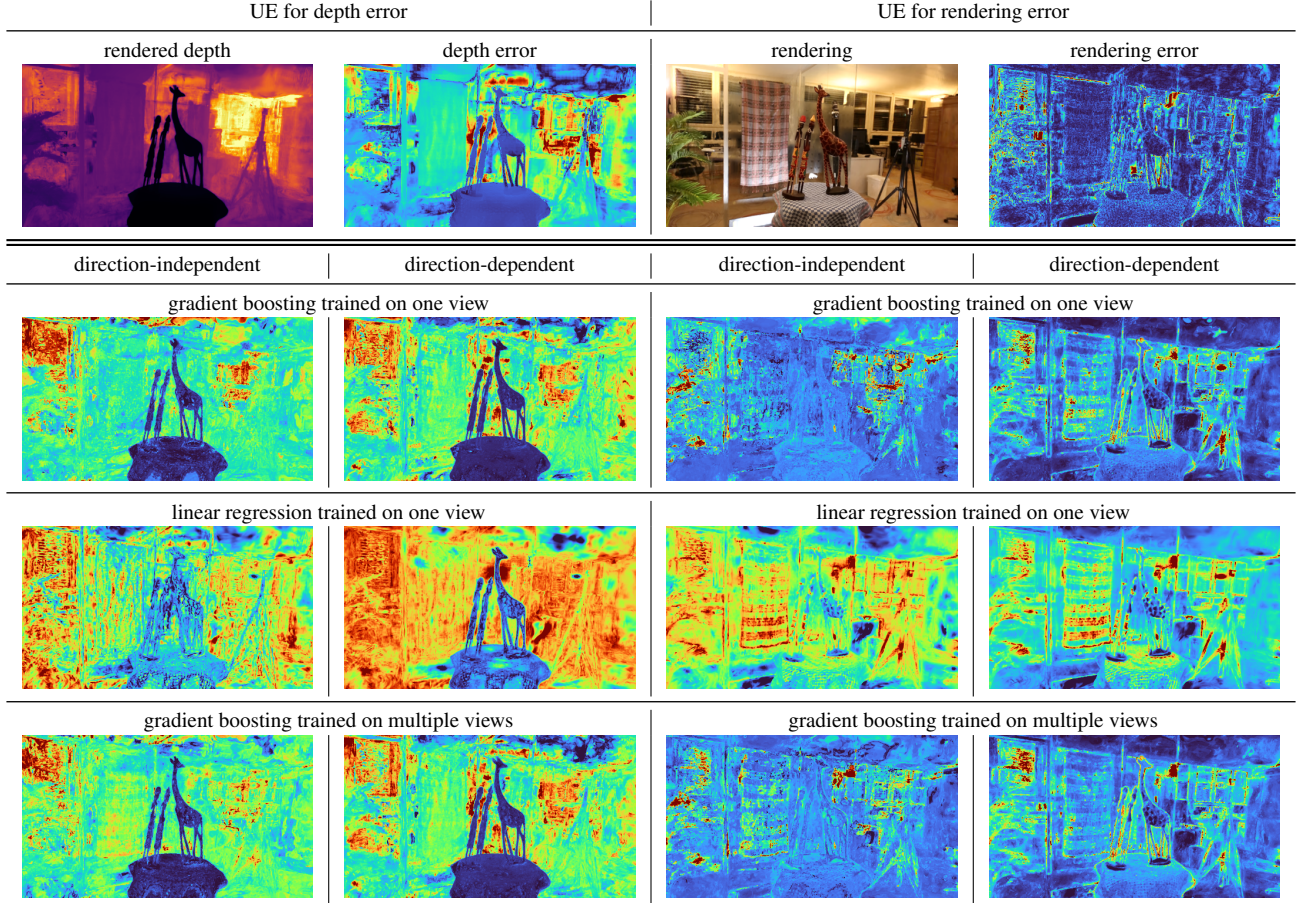


Figure 4. Qualitative example of the UE of our method for the scene africa of the LF dataset. Top row depth and color renderings of view and their error maps. Below predicted error from different regression models trained on direction-independent or direction-dependent (plus FoV counter) uncertainty feature maps.

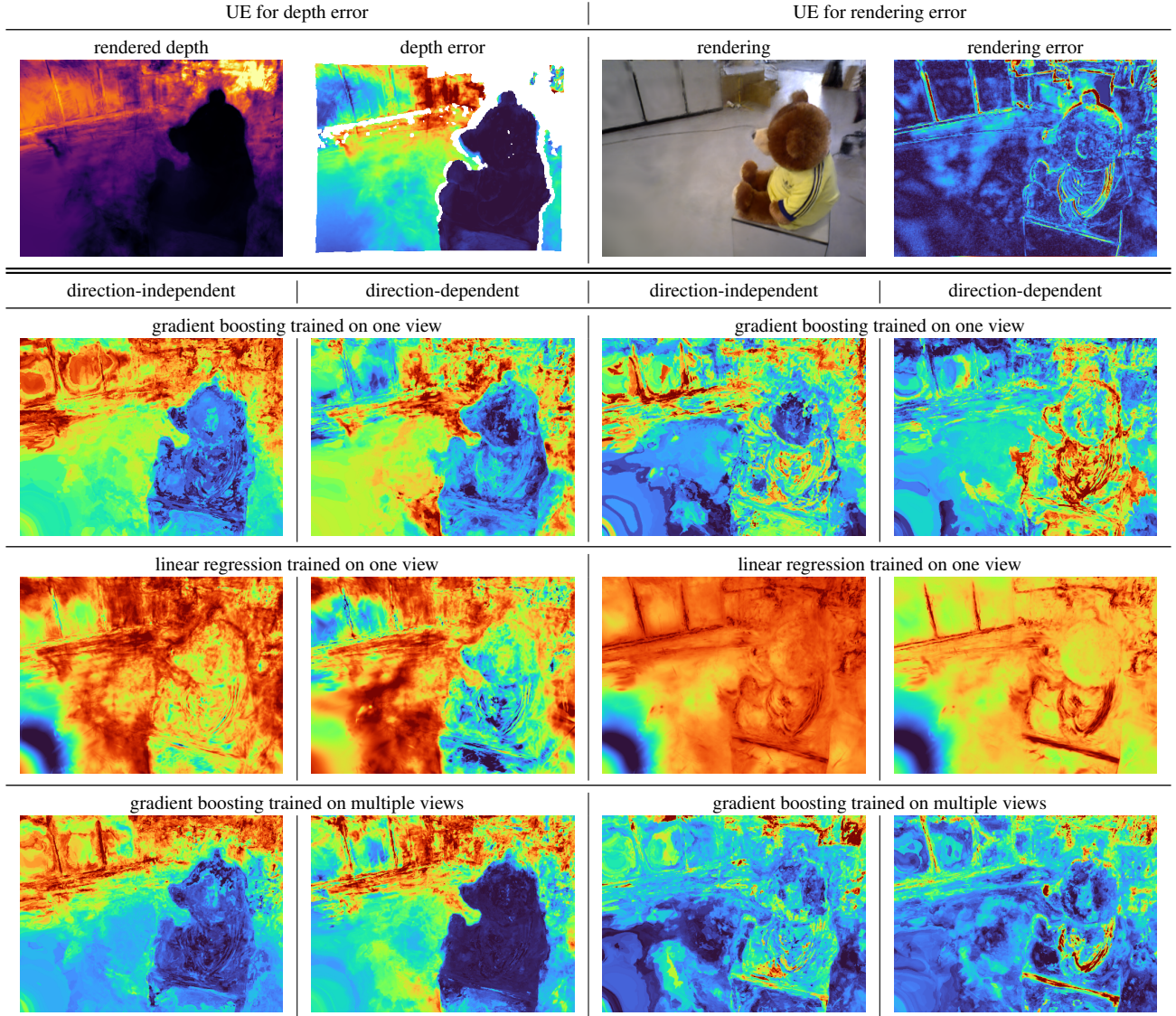


Figure 5. Qualitative example of the UE of our method for the scene teddy2 of the TUM dataset. Top row depth and color renderings of view and their error maps. Below predicted error from different regression models trained on direction-independent or direction-dependent (plus FoV counter) uncertainty feature maps.